NASA TECHNICAL MEMORANDUM

NASA TM X-2925

NASA TM X-2925

ANALYZING THE THERMIONIC REACTOR CRITICAL EXPERIMENTS

by George F. Niederauer

Lewis Research Center
Cleveland, Ohio 44135

NATIONAL AERONAUTICS AND SPACE ADMINISTRATION • WASHINGTON, D. C. • NOVEMBER 1973

1. Report No.	2. Government Accession No.	3. Recipient's Catalog No.
NASA TM X-2925		

4. Title and Subtitle	5. Report Date
ANALYZING THE THERMIONIC REACTOR CRITICAL EXPERIMENTS	November 1973
	6. Performing Organization Code
7. Author(s)	8. Performing Organization Report No.
George F. Niederauer	E-7517
	10. Work Unit No.
9. Performing Organization Name and Address	503-25
Lewis Research Center National Aeronautics and Space Administration Cleveland, Ohio 44135	11. Contract or Grant No.
	13. Type of Report and Period Covered
12. Sponsoring Agency Name and Address	Technical Memorandum
National Aeronautics and Space Administration Washington, D. C. 20546	14. Sponsoring Agency Code

15. Supplementary Notes

16. Abstract

The Thermionic Reactor Critical Experiments (TRCE) consisted of fast-spectrum highly enriched U^{235} cores reflected by different thicknesses of beryllium or beryllium oxide with a transition zone of stainless steel between the core and reflector. The mixed fast-thermal spectrum at the core-reflector interface region poses a difficult neutron transport calculation. Calculations of TRCE using ENDF/B fast-spectrum data and GATHER libary thermal-spectrum data agreed within about 1 percent for the multiplication factor and within 6 to 8 percent for the power peaks. Use of GAM libary fast-spectrum data yielded larger deviations. The results were obtained from DOT Rθ calculations with leakage cross sections, by region and by group, extracted from DOT RZ calculations. Delineation of the power peaks required extraordinarily fine mesh size at the core-reflector interface.

17. Key Words (Suggested by Author(s))	18. Distribution Statement
Nuclear reactors Critical experiments Two-dimensional transport calculations Beryllium-reflected fast spectrum cores	Unclassified - unlimited

19. Security Classif. (of this report)	20. Security Classif. (of this page)	21. No. of Pages	22. Price*
Unclassified	Unclassified	44	Domestic, $3.00 Foreign, $5.50

* For sale by the National Technical Information Service, Springfield, Virginia 22151

ANALYZING THE THERMIONIC REACTOR CRITICAL EXPERIMENTS

by George F. Niederauer

Lewis Research Center

SUMMARY

In the Thermionic Reactor Critical Experiments (TRCE), neutron multiplication and power distributions in a series of moderator-reflected fast-spectrum reactors were measured. TRCE consisted of hexagonal configurations of highly enriched uranium-235 (U^{235}), cores reflected by different thicknesses of beryllium or beryllium oxide, with a transition zone of stainless steel between the core and reflector.

Multigroup calculations of TRCE used the cross-section libraries GAM and ENDF/B in the fast region and GATHER in the thermal region. The mixed fast-thermal spectrum at the core-reflector interface region posed a difficult neutron transport calculation. Two-dimensional RZ and Rθ models were calculated by DOT and one-dimensional models by ANISN. Transverse leakage was treated by using either an effective buckling height H_B or effective leakage cross sections Σ_L. The latter were divided by region and by energy group, and thus gave more accurate results.

The measured and calculated values of the multiplication factors using ENDF/B data were compared and agreed within about 1 percent in reactivity when leakage cross sections were used, but deviated 3 to 4 percent in reactivity when a buckling height was used. Using GAM data in place of ENDF/B gave larger deviations.

The measured and calculated power peaks at the hexagonal core-reflector interfaces normalized to the power at the center of the core were also compared. The measured peak at the center-of-the-flat region for a Be-reflected core was 3.75±0.20 and was calculated to be 3.45 by using transverse leakage cross sections Σ_L. Comparably good agreement was obtained for BeO reflectors and at the apex-of-flat interface locations. Delineation of the power peaks required extraordinarily fine mesh sizes at the core-reflector interface.

INTRODUCTION

The Thermionic Reactor Critical Experiments (TRCE) were performed at the Low

Power Test Facility in Idaho from January to March of 1966. The TRCE reactor was a small, compact, uniformly reflected, hexagonal, fast-spectrum reactor with moderating reflectors (ref. 1). It is well suited to an experimental check of the data and methods used in reactor neutronics calculations of small, fast reactors. The mixed fast-thermal neutron spectrum at the core-reflector interfaces poses a difficult transport calculation.

Many of the neutronics calculations at the Lewis Research Center have been based on the nuclear cross-section data contained in the libraries of the GAM (ref. 2) and GATHER (ref. 3) codes. Several years ago nearly every installation which performed neutronics calculations had its own data base for nuclear cross sections. Although some libraries were shared between installations, most of the data bases were different from one another as a result of revising and updating according to individual needs. Recently, the introduction of national neutron-cross-section standards has changed the data base for reactor neutronics calculations markedly. The national standard library of nuclear cross sections, the Evaluated Nuclear Data Files (ENDF, refs. 4 and 5), may eventually be the data base for everyone.

This report documents the accuracy of using the latest ENDF cross sections, version ENDF/B III wherever possible, and recently developed cross-section computer codes that are more sophisticated than codes previously used. Specifically, a preprocessing code GAND (ref. 6) is used that interfaces with the ENDF library and with the fast-cross-section codes GAF/GAR (ref. 7 and 8). The GAF/GAR codes, GAF for the region above the resolved resonances and GAR for the resonance region, which replace GAM, have, among other improvements, the ability to consider explicitly the possible overlap effects between resonances of a resonance absorber and of mixtures of resonance absorbers (ref. 6).

Two configurations of TRCE and two moderating reflectors are examined in this report. Configurations referred to as B1 and B2 are beryllium-reflected cores, with the only difference between them being the smaller thickness of the radial reflector in the B2 configuration. The B1 configuration is also examined with a beryllium-oxide (BeO) radial reflector.

This report covers the following topics, in the order of their presentation: the physical description of the TRCE assembly; modeling of the TRCE in one-dimensional radial geometry and in two-dimensional RZ and Rθ geometries; results of the multigroup transport calculations; and a discussion of representative results.

PHYSICAL DESCRIPTION OF THERMIONIC REACTOR CRITICAL EXPERIMENT

Geometry

The configurations for the Thermionic Reactor Critical Experiment were assembled in the split-table critical experiment used in the 710 reactor program (ref. 9). The table consists of horizontal rows of hexagonal aluminum tubes which form a honeycomb structure. The aluminum tubes with 0.079-centimeter (0.031-in.) thick walls have a nominal manufactured outside diameter across the flats of 4.445 centimeters (1.750 in.), but the nominal spacing of the assembled tubes is 4.465 centimeters (1.758 in.) (ref. 10). The tubes take up about 7 percent of the available volume.

A layout across the assembly tubes of the B1 configuration is shown in figure 1. Basically, the TRCE B1 configuration consists of a 31-centimeter (12-in.) wide by 37-centimeter (15-in.) long hexagonal core composed of highly enriched uranium-235 (U^{235}), tungsten trioxide (WO_3), aluminum oxide (Al_2O_3), nickel, and stainless steel. It is reflected by 16 centimeters (6 in.) of beryllium and has a stainless-steel transition region between the core and radial reflector. The B2 configuration differs from the B1 by a smaller radial reflector, 9 centimeters (3.5 in.) thick.

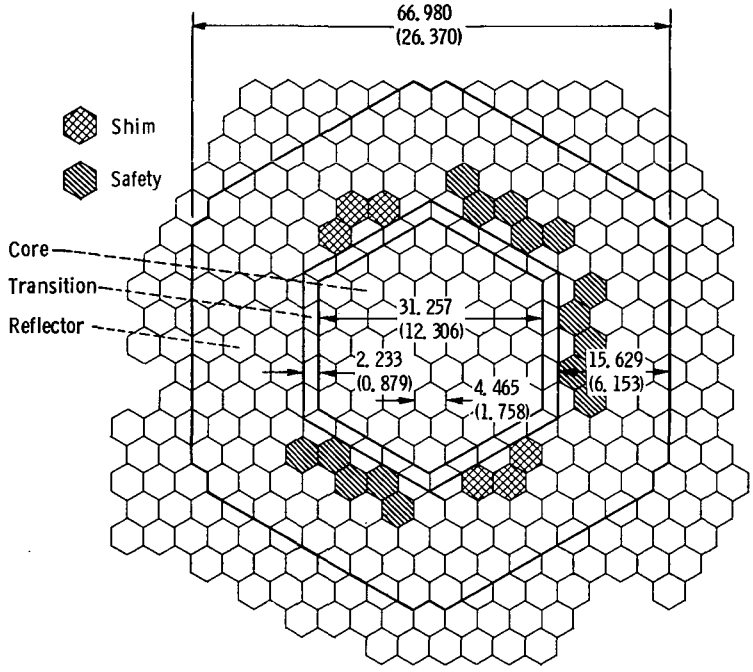

Figure 1. - Crosswise layout of B1 configuration. (Dimensions are in cm (in.).)

Consider a "hex" as the distance across the flat of one of the aluminum tubes, about 4.4 centimeters (1.75 in.). The B1 reflector is three and one-half "hexes" thick, and the B2 reflector is two "hexes" thick. In both cases, the outer corners of the reflector are missing one-third hex from forming a hexagonal outer boundary. Thirty hex bars (15 in each table half) controlled by six actuators (three in each table half) were used as safety control rods. Twelve hex bars (six in each table half) controlled by four actuators (two in each table half) were used as shim rods.

A layout along the length of the reactor is shown in figure 2. The widths are taken across the flats of the hexagonal boundaries. Except for the 3.15-centimeter protrusion of the radial reflector below the lower axial reflector, the reactor is symmetric about its central plane.

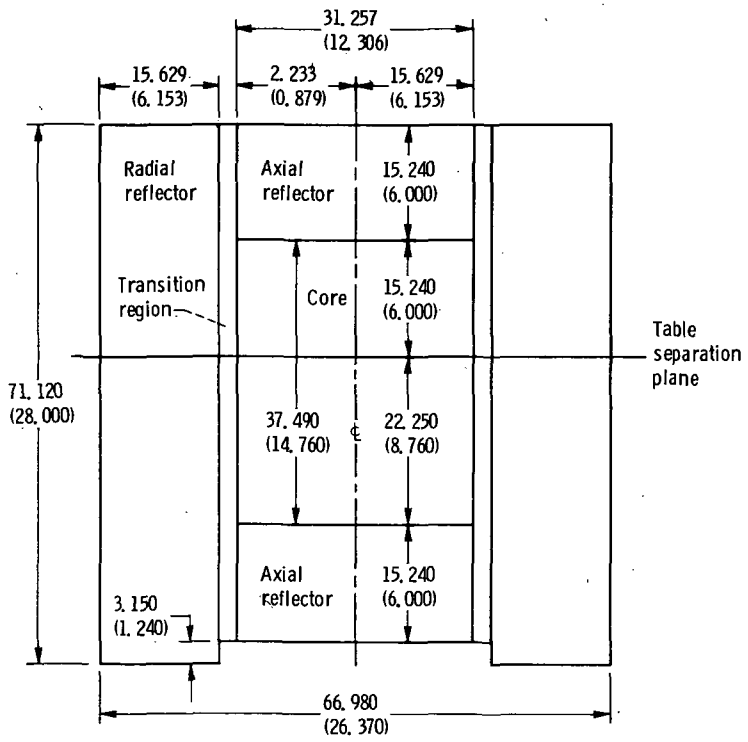

Figure 2. - Lengthwise layout for B1 configuration. (Dimensions are in cm (in.).)

Although the materials were placed in the honeycomb structure as individual small pieces of oralloy, stainless steel, or WO_3, they were evenly distributed so that the overall effect was a homogeneous region. Most of the materials in the core and transition region were contained in rods from 0.432 to 0.476 centimeter (0.17 to 0.1875 in.) in diameter. Some stainless steel in the core was in 0.318-centimeter (0.125-in.) diameter rods and 0.015-centimeter (0.006-in.) thick plates. A sample core hex loading is shown in figure 3. In the transition region, stainless steel was inserted as rods and tubes with aluminum sheets separating the rows of stainless steel, as shown in figure 4. Beryllium was loaded into the reflectors mainly in the form of full and half hexes.

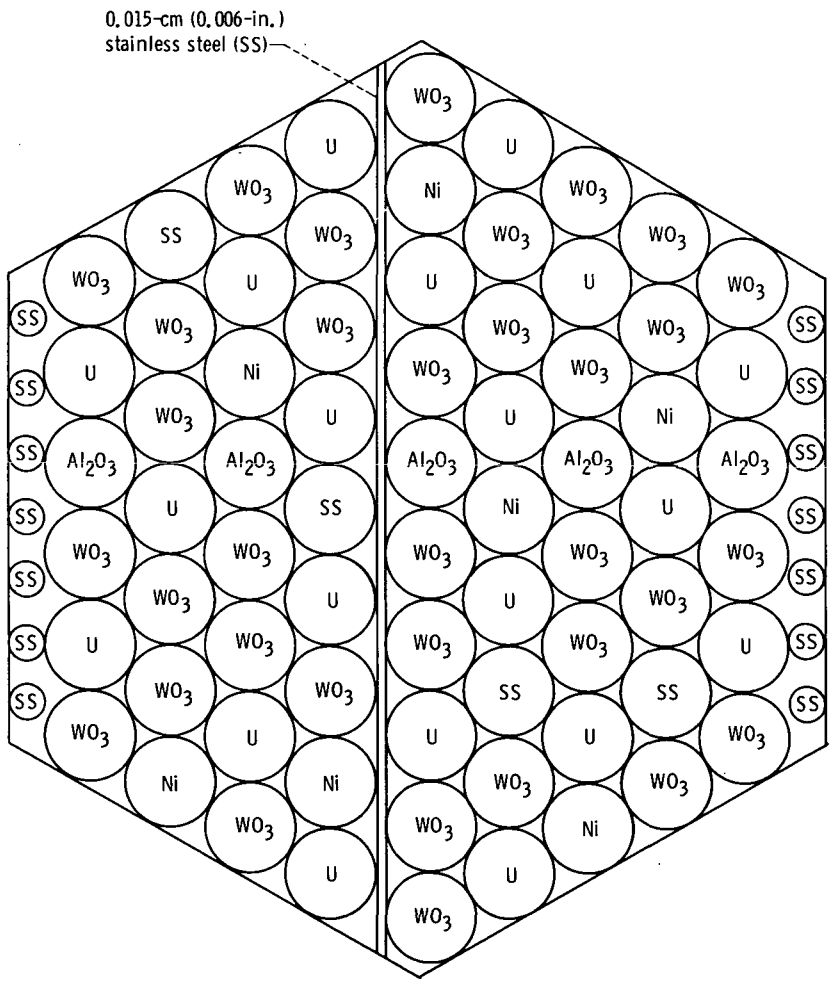

Figure 3. - Typical core cell loading pattern, shown by fixed table half. (From ref. 1.)

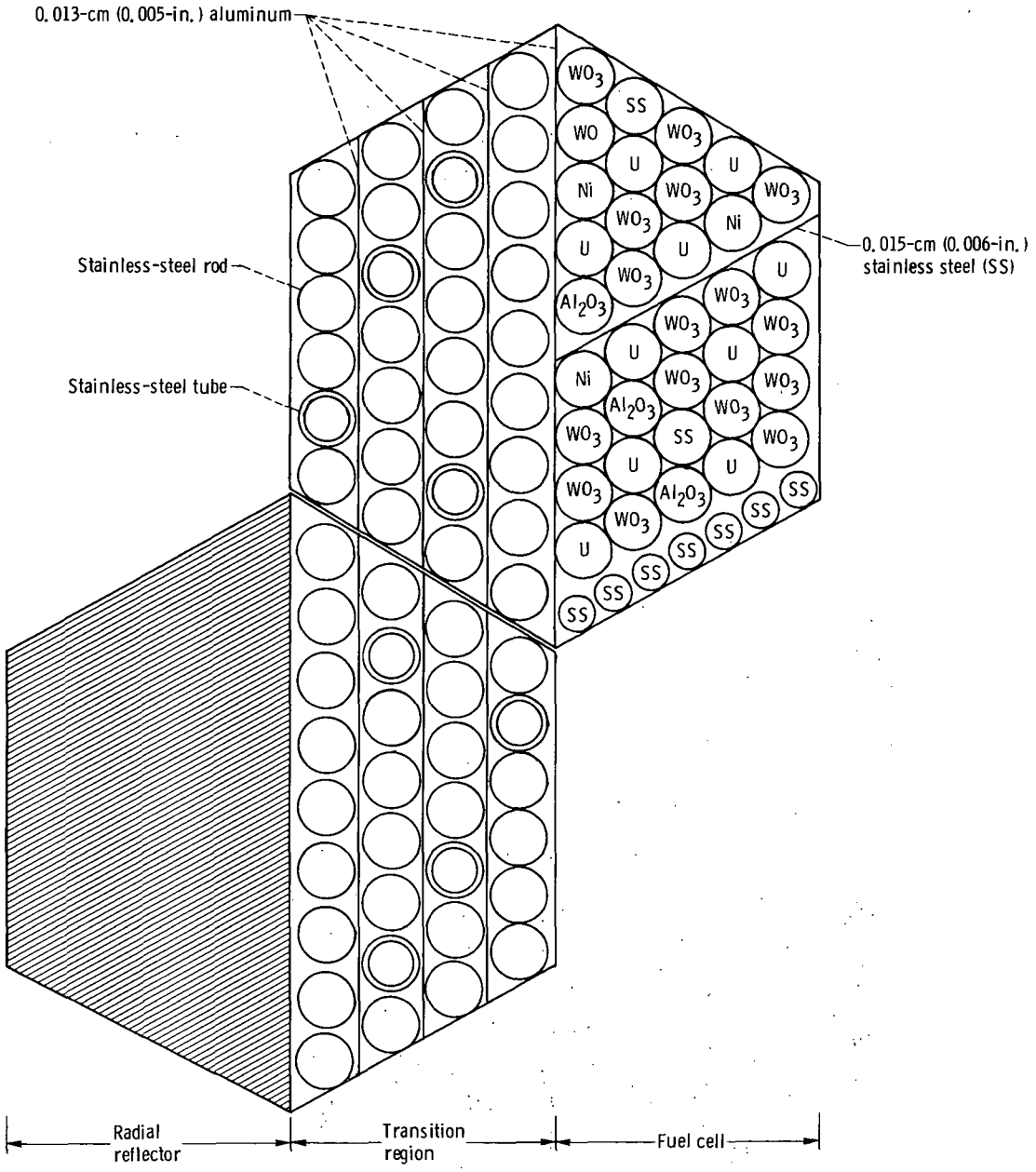

Figure 4. - Typical transition-region cell loading pattern, shown by fixed table half. (From ref. 1.)

Materials

Measured weights are available for most of the materials in TRCE. All the weights for the core and axial reflector materials are available from GEMP-423 (ref. 1) or the reactor log, but derived volume fraction data must be relied upon for materials in the other regions. Cross checking the data within GEMP-423 and with the reactor log has led to the following tables as the best information available.

The material inventories in the B1 and B2 cores are listed in table 1. Wherever possible, the atom densities were calculated directly from the mass per piece and from

TABLE 1. - B1 AND B2 CORE MATERIAL INVENTORY

Material	Number of rods or pieces	Element or isotope	Rod diameter		Rod mass, g	Core mass[a], kg	Volume fraction[a]	Atom density[a], atoms/(b)(cm)
			cm	in.				
B1 core								
Oralloy	1007	U^{234} U^{235} U^{236} U^{238}	0.432	0.17	102.25	102.97	0.1743	0.000082 .007751 .000043 .000437
WO_3	1666	W O	0.457	0.18	42.36	70.57	0.3233	0.005779 .017338
Al_2O_3	224	Al O	0.476	0.1875	24.19	5.42	0.0472	0.006221 .020364
Al	49	Al					0.0698	0.004203
Ni	343	Ni	0.476	0.1875	58.55	20.08	0.0722	0.006495
Stainless steel	196 686 43	Cr Fe Ni	0.476 .318 [b].015	0.1875 .125 [b].006	52.59 23.29	10.31 15.98	0.0413 .0642 .0043	0.001898 .006652 .000841
B2 core (where different from B1 core)								
Oralloy	1131	U^{234} U^{235} U^{236} U^{238}	0.432	0.17	102.25	113.64	0.1957	0.000092 .008705 .000049 .000491
Al_2O_3	100	Al O	0.476	0.1875	24.19	2.42	0.0211	0.005104 .018689

[a]Derived quantity.

[b]Plate thickness.

the number of pieces of a given material. This was possible for all materials in the core, except for stainless steel because there were no measured masses for the plates.

The volume fraction of stainless steel in the plates was estimated from the size of plate shown in figure 3; the 0.0043 estimate was in agreement with the estimate sent in a private communication by J. F. Kunze of Aerojet Nuclear Company (AGN) in 1972. Along with a lack of precision in the volume fraction of stainless steel is the lack of a According to Kunze, all stainless steel used in TRCE is type 304. The AISI composition limits (ref. 10) for type 304 stainless steel are listed in table 2, along with the assumed composition for TRCE. Only the three major components were kept for the calculations reported herein.

TABLE 2. - COMPOSITION OF TYPE

304 STAINLESS STEEL

Element	Composition, wt. %	
	AISI limits[a]	TRCE
Fe	----------	71.5
Cr	18 to 20	19
Ni	8 to 11	9.5
C	0 to 0.08	0
Mn	0 to 2	↓
Si	0 to 1	
S	0 to 0.03	
P	0 to 0.045	

[a]AISI composition limits in wt. % of wrought stainless steel, type 304, from ref. 10.

There is a disagreement between the volume fractions listed in table 1 and those listed in table II.2 of reference 1. The volume fractions in table 1 were based on the dimensions of rods and pieces that are also listed in table 1. The volume fractions in table II.2 of reference 1 were calculated from the measured mass and an assumed density. For example, with the given mass of oralloy and an assumed density of 18.7 g/cm^3, the volume fraction of oralloy is 0.1736; whereas, the given mass and rod dimensions lead to a 0.1743-volume fraction.

Reference 1 is not precise on the mass of aluminum contained in the hexagonal aluminum boxes, and there is a discrepancy within the report on the volume fraction of aluminum in the honeycomb structure. In a private communication, Kunze wrote that the actual weight of the aluminum tubes is 99.1 grams per linear foot, and this value is

used herein. This results in a slightly higher (0.4203×10^{22} as compared to 0.417×10^{22} atoms/cm^3) atom density for aluminum than that reported in GEMP-423 (ref. 1).

The oralloy fuel used in TRCE was analyzed for isotopic composition. The results are listed in table 3, along with the atomic weights of the isotopes. In the calculations of TRCE, only the two most predominant of these isotopes, U^{235} and U^{238}, are included.

TABLE 3. - COMPOSITION OF ORALLOY

Isotope	Composition	
	Weight percent	Atomic weight
U^{234}	0.98	234.0409
U^{235}	93.18	235.0435
U^{236}	.52	236.0456
U^{238}	5.32	238.0508

The masses of U^{234} and U^{236} isotopes are represented by U^{238}. Core B2 had 1131 oralloy rods according to table II.2 (p. 25 of ref. 1) and 1135 rods according to page 104 of reference 1. A check in the reactor log confirmed that the 1131 listing is the correct one (private communication from Kunze).

The axial reflector is composed of partial hex pieces of beryllium and rods and tubes of stainless steel, as shown in figures 5 to 7. The axial reflector layout is shown in figure 8. The atom densities for all the materials in this region were calculated from the measured weights of the materials. The beryllium pieces averaged 306.95 grams per hexagonal cell. Stainless steel in the reflector was in two forms: 0.476-centimeter (0.1875-in.) diameter rods, and tubes of the same outside diameter and 0.425-centimeter (0.1675-in.) inside diameter. The number of pieces and reflector masses are listed in table 4 for one of the two axial reflectors.

Neither numbers of pieces nor weights are given for the materials in the transition region; only the volume fractions are listed. Only two materials, aluminum and stainless steel, are used in this region, but there are aluminum spacers separating the rows of stainless-steel rods and tubes. By using the published value (2.699 g/cm^3) for the density of aluminum (ref. 10), it can be verified that the hex boxes (4.465 cm (1.758 in.) across the flats, with 0.079-cm (0.031-in.) thick walls) have an atom density of 0.00417 atoms per barn per centimeter, in agreement with GEMP-423 (ref. 1). With this value

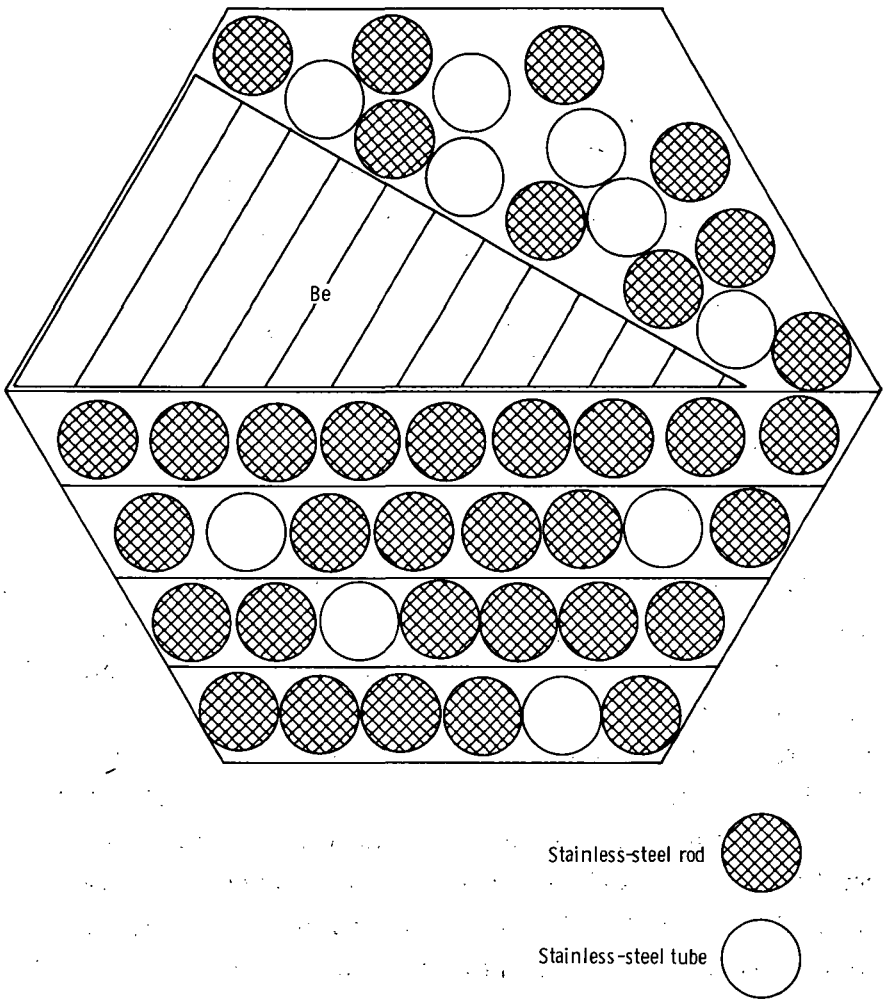

Figure 5. - Axial reflector - transition region cell loading pattern. (From ref. 1.)

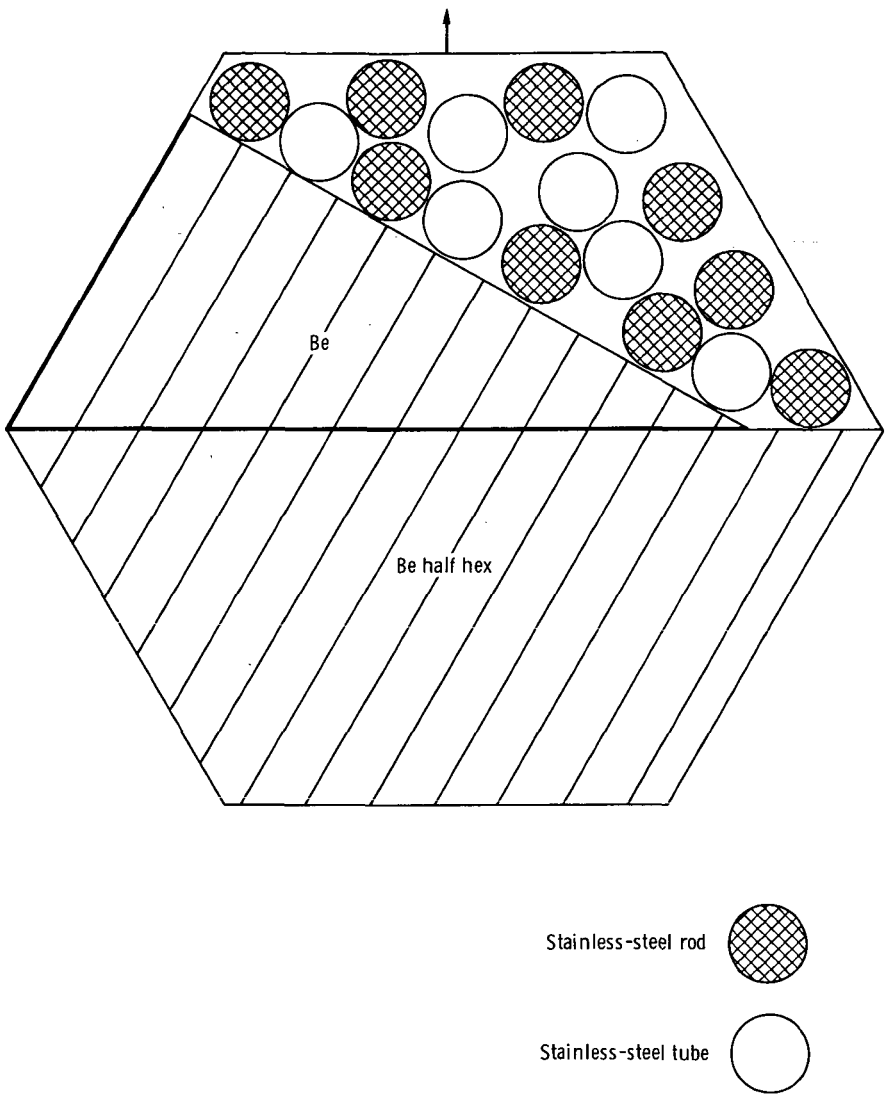

Figure 6. - Axial reflector - type A cell loading pattern. (From ref. 1.)

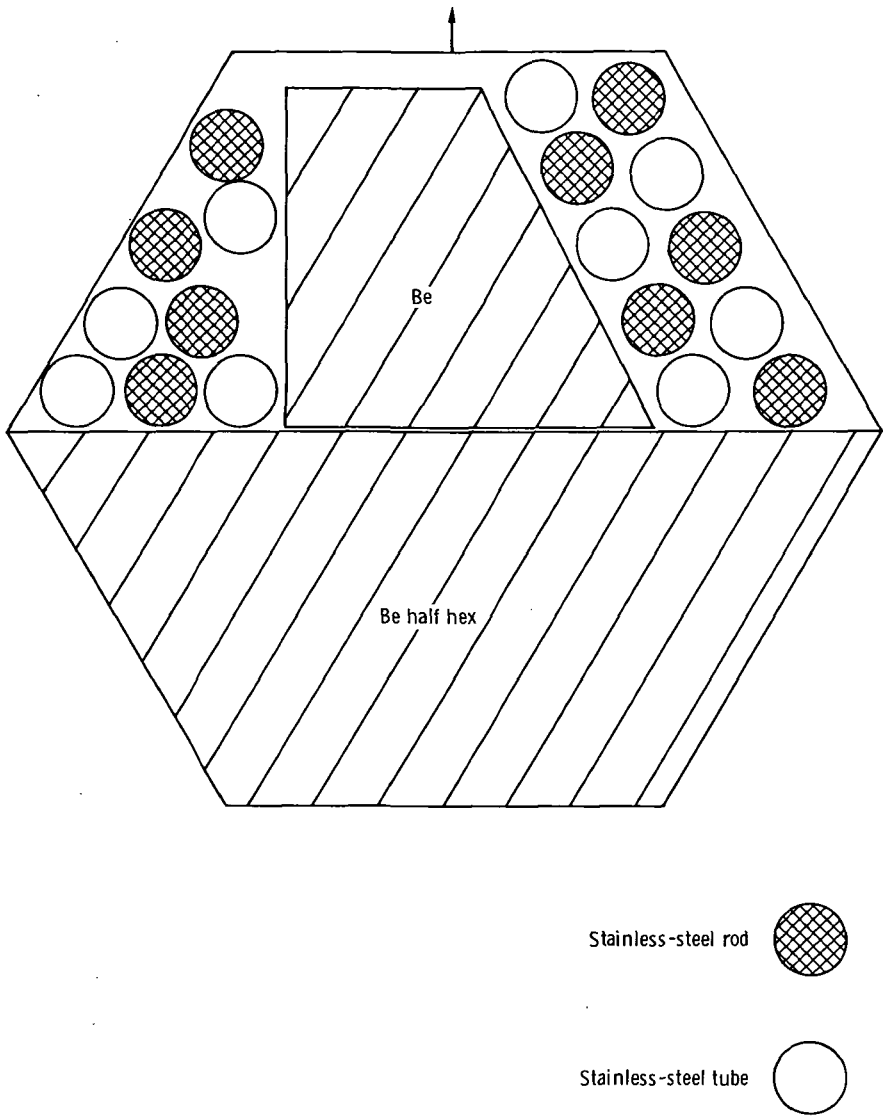

Figure 7. - Axial reflector - type B cell loading pattern. (From ref. 1.)

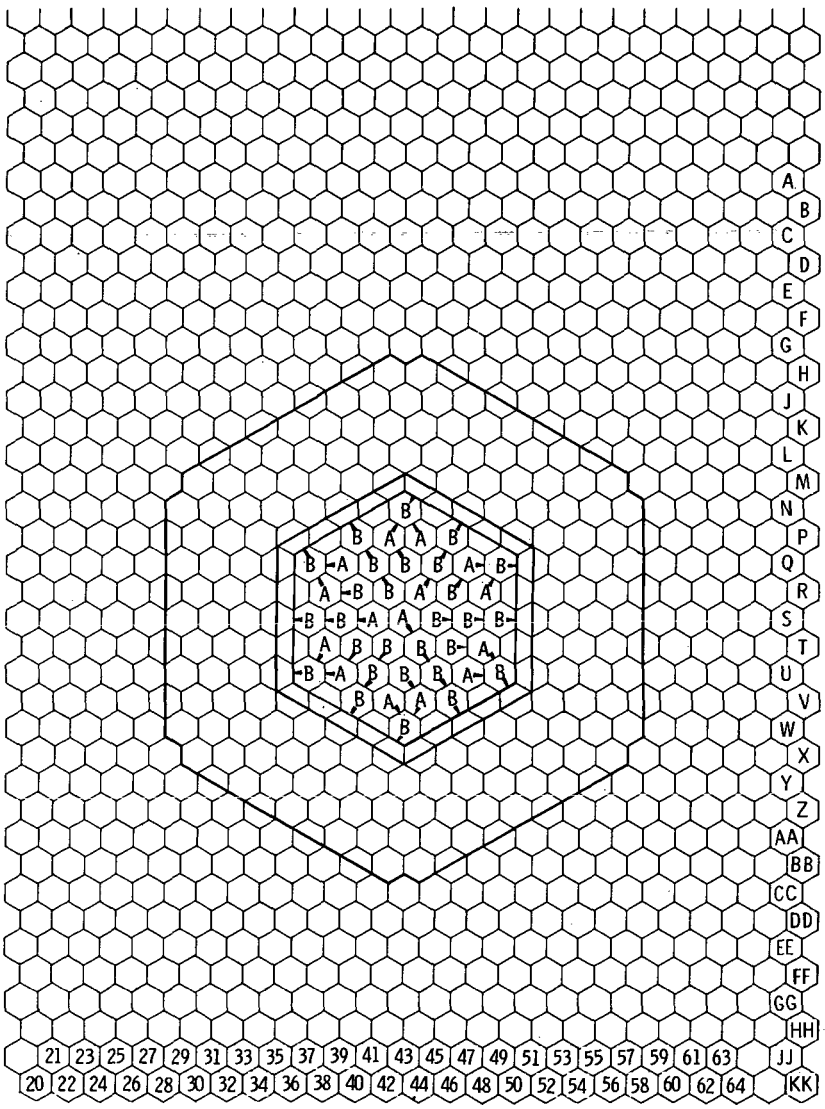

Figure 8. - Axial reflector layout, shown by fixed table half. The A and B denote the type of end reflector (figs. 6 and 7); the arrows show the orientation of the end reflector cells. (From ref. 1.)

TABLE 4. - AXIAL-REFLECTOR MATERIAL INVENTORY

Material	Number of pieces	Piece description	Piece mass, g	Reflector mass[a], kg	Volume fraction[a]	Element	Atom density[a], atoms/(b)(cm)
Be	21 28 43	Triangle 1/4 Hex 1/2 Hex	116.38 95.87 203.94	[b]15.04		Be	0.078634
Al	49	Hex tube	99.1	4.86	0.0698	Al	0.004203
Stainless steel	441 343	Rod[c] Tube[d]	21.38 4.24	10.88		Cr Fe Ni	0.001857 .000822 .006508

[a]Derived quantity.

[b]Based on average weight of 306.95 g per hexagonal cell.

[c]0.476 cm (0.1875 in.) diameter.

[d]0.476 cm (0.1875 in.) outside diameter and 0.425 cm (0.1675 in.) inside diameter.

for the aluminum density and the value for stainless-steel density of 7.98 g/cm^3 used by Kunze, the inventory of materials in the transition region (table 5) is derived.

As in the case of the transition region, no count of pieces nor list of weights was published for the radial reflectors. In GEMP-423 (ref. 1) the volume fraction of beryllium in both the B1 and B2 radial reflectors is listed as 0.87. However, Sawyer (ref. 11) lists updated volume fractions as 0.881 for the B1 reflector and 0.873 for the B2 reflector. This matter could not be resolved any further, so the latter values are assumed to be the best available information. The B1 and B2 radial reflector material inventories for a beryllium density of 1.85 g/cm^3 are listed in table 6.

Besides examining the B1 and B2 configurations, differences between beryllium- and beryllium-oxide-reflected cores were investigated. In TRCE the measurement of the effect of reflector material substitution was determined by substituting beryllium oxide for beryllium in a 60° sector of the radial reflector of configuration A. However, other differences between configurations A and B are of second order compared to the difference in the reflector material substitution.

To accomplish the measurement, 49 658 grams of beryllium were replaced by 78 605 grams of beryllium oxide in a 60° sector of the radial reflector. If we assume that this resulted in no change in the volume fraction of the reflecting material, the ratio of the effective density of the beryllium oxide to the beryllium is 1.58, resulting in a 2.93-g/cm^3 density for beryllium oxide. But, the nominal density of beryllium oxide is 2.85 g/cm^3; therefore, calculations were made for both densities first, to compare calculation with experiment and, second, to compare the effectiveness

TABLE 5. - TRANSITION-REGION MATERIAL INVENTORY

Material	Volume fraction[a]	Element	Atom density[b], atoms/(b)(cm)
Al	0.094	Al	0.005664
Stainless steel	0.553	Cr	0.009710
		Fe	.004310
		Ni	.034027

[a]Reported quantity.
[b]Derived quantity.

TABLE 6. - B1 AND B2 RADIAL-REFLECTOR MATERIAL INVENTORY

Configuration	Material	Volume fraction	Atom density, atoms/(b)(cm)
B1	Be	[a]0.881	0.108916
	Al	[b].0698	.004203
B2	Be	[a]0.873	0.107927
	Al	[b].0698	.004203

[a]From ref. 11
[b]Based on 99.1 g/linear foot.

TABLE 7. - BERYLLIUM-OXIDE-RADIAL-REFLECTOR MATERIAL INVENTORY

BeO density, g/cm^3	Material	Volume fraction	Element	Atom density, atoms/(b)(cm)
2.93	BeO	0.881	Be	0.062123
			O	.062123
	Al	.0698	Al	.004203
2.85	BeO	0.881	Be	0.060460
			O	.060460
	Al	.0698	Al	.004203

of beryllium and beryllium oxide on a common-volume fraction basis. The material inventories of the beryllium oxide reflectors are given in table 7.

MODELING THE THERMIONIC REACTOR CRITICAL EXPERIMENT

Choosing and developing mathematical models of a real reactor are influenced by the physical quantities under investigation and the pecularities of the reactor under study. The two physical quantities under closest scrutiny in these calculations are the multiplication factor k and the power peaks. A peculiarity of this reactor which has great influence on details of the model is the interface between the fast and thermal spectrums at the core edge. The mixing of the two spectrums leads to large power gradients, as measured in the critical experiments, and requires special consideration in the model.

Cross Sections

Values of fast cross sections were derived from two basic sources: the GAM library and the ENDF/B library; thermal cross sections were provided by the GATHER library. One set of calculations of TRCE involved the GAM/GATHER data. A second - and the most extensive - set of calculations involved as much as the ENDF/B III data as could be processed through GAND/GAF/GAR for the fast region (everything but stainless steel) and GATHER data for the thermal region. The sources for the fast cross sections for the latter (and primary) set are listed in table 8. All these cross sections

TABLE 8. - LIBRARY SOURCES FOR PRIMARY SET OF FAST CROSS SECTIONS

Material	Library	MAT number
Be	ENDF/B II	1007 or 1154
O	ENDF/B III	1134
Al	ENDF/B III	1135
Cr	GAM	24
Fe	GAM	26
Ni	GAM	28
W^{182}	ENDF/B III	1060
W^{183}	↓	1061
W^{184}		1062
W^{186}		1063
U^{235}		1157
U^{238}		1158

came from the ENDF/B III library (ref. 12), except for beryllium and stainless steel (chromium, iron, and nickel) due to an incompatibility between ENDF/B II and GAND/GAF/GAR for these materials. (ENDF/B does not list all resonance data over the same energy range for all materials, but GAF/GAR requires it.) In this case, the beryllium cross sections were obtained from the ENDF/B II library (ref. 13) through GAND/GAF/GAR, and the stainless-steel cross sections were obtained from GAM.

Using SUPERTOG (ref. 14) to reduce the ENDF/B data to the GAM library format enabled the use of all ENDF/B III cross sections except that for stainless steel. The final microscopic cross sections were obtained through GAM rather than through GAF/GAR. Two calculations were performed with this third set to detect differences in ENDF/B II (MAT 1007) and ENDF/B III (MAT 1154) beryllium cross sections.

Energy Structure

Two energy structures were chosen for the calculations. The primary set contained 13 fast and nine thermal groups in a 22-group set; the other set contained 35 groups, with 26 of them fast. In both sets the boundary between fast and thermal was set at 0.414 eV. The upper energy and lethargy boundaries, along with their midpoints, are listed in table 9 for the 22-group set and in table 10 for the 35-group set.

TABLE 9. - ENERGY STRUCTURE FOR 22 GROUPS

Group	Upper boundary		Midpoint	
	Energy	Lethargy	Energy	Lethargy
1	14.92 MeV	-0.4	7.41 MeV	0.3
2	3.68 MeV	1.0	2.86 MeV	1.25
3	2.23 MeV	1.5	1.738 MeV	1.75
4	1.353 MeV	2.0	1.054 MeV	2.25
5	821 keV	2.5	639 keV	2.75
6	498 keV	3.0	302 keV	3.5
7	183.2 keV	4.0	142.6 keV	4.25
8	111.1 keV	4.5	67.4 keV	5.0
9	40.9 keV	5.5	24.8 keV	6.0
10	15.03 keV	6.5	9.12 keV	7.0
11	5.53 keV	7.5	2.03 keV	8.5
12	749 eV	9.5	243 eV	10.62
13	78.9 eV	11.75	5.72 eV	14.38
14	.414 eV	17.0	.288 eV	17.36
15	.200 eV	17.73	.167 eV	17.91
16	.140 eV	18.08	.118 eV	18.25
17	.100 eV	18.42	.0837 eV	18.60
18	.070 eV	18.78	.0529 eV	19.06
19	.040 eV	19.34	.0283 eV	19.68
20	.020 eV	20.03	.0141 eV	20.38
21	.010 eV	20.72	.0063 eV	21.18
22	.004 eV	21.64	----------	-----

TABLE 10. - ENERGY STRUCTURE FOR 35 GROUPS

Group	Upper boundary		Midpoint	
	Energy	Lethargy	Energy	Lethargy
1	14.92 MeV	-0.4	11.62 MeV	-0.15
2	9.05 MeV	.1	7.05 MeV	.35
3	5.49 MeV	.6	4.27 MeV	.85
4	3.33 MeV	1.1	2.59 MeV	1.35
5	2.02 MeV	1.6	1.572 MeV	1.85
6	1.225 MeV	2.1	954 keV	2.35
7	742 keV	2.6	550 keV	2.90
8	408 keV	3.2	302 keV	3.50
9	224 keV	3.8	165.7 keV	4.10
10	122.8 keV	4.4	91.0 keV	4.70
11	67.4 keV	5.0	46.3 keV	5.375
12	31.8 keV	5.75	21.9 keV	6.125
13	15.03 keV	6.50	10.33 keV	6.875
14	7.10 keV	7.25	4.88 keV	7.625
15	3.35 keV	8.00	2.31 keV	8.375
16	1.585 keV	8.75	1.089 keV	9.125
17	749 eV	9.50	514 eV	9.875
18	354 eV	10.25	243 eV	10.625
19	167.0 eV	11.00	114.8 eV	11.375
20	78.9 eV	11.75	54.2 eV	12.125
21	37.3 eV	12.50	25.6 eV	12.875
22	17.60 eV	13.25	12.10 eV	13.625
23	8.32 eV	14.00	5.72 eV	14.375
24	3.93 eV	14.75	2.70 eV	15.125
25	1.855 eV	15.50	1.275 eV	15.875
26	.876 eV	16.25	.602 eV	16.625
27	.414 eV	17.00	.288 eV	17.36
28	.200 eV	17.73	.167 eV	17.91
29	.140 eV	18.08	.118 eV	18.25
30	.100 eV	18.42	.0837 eV	18.60
31	.070 eV	18.78	.0529 eV	19.06
32	.040 eV	19.34	.0283 eV	19.68
33	.020 eV	20.03	.0141 eV	20.38
34	.010 eV	20.72	.0063 eV	21.18
35	.004 eV	21.64	----------	------

Model Geometry

The critical assembly is slightly asymmetric in the axial direction because the radial reflector protrudes beyond the plane of the axial reflector at one end of the assembly and not at the other. The geometry of the critical assembly was compromised by including the protrusion at both ends of the assembly. Thus, the RZ geometry can then be represented by the half-assembly model shown in figure 9. The

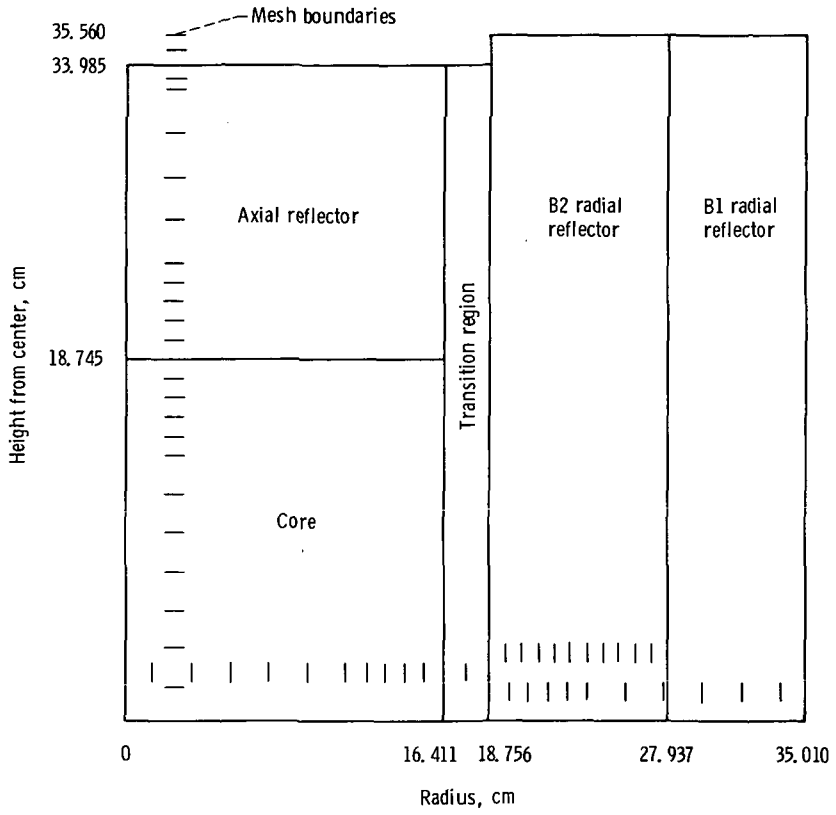

Figure 9. - RZ model geometry.

24 radial and 25 axial mesh intervals are shown in figure 9. The RZ model is fairly coarse, as characterized by the 1-centimeter mesh interval, which is too large to reveal the power peak at the core outer boundaries.

In the Rθ plane through the core, TRCE has a reflective symmetry about the 30^{o} sector of the hexagon shown in figure 10. The computer model geometry, which overlies the actual assembly geometry in figure 10, has a fine mesh built into it to define the power peaks at two locations along the core-transition boundary: at the apex of the flat and midway between the apexes, or center-of-the-flat location. The Rθ model has 12 azimuthal and 67 radial mesh intervals, as shown in figure 10. An example of the fineness of the mesh is the 0.001-centimeter interval at the core-transition boundary.

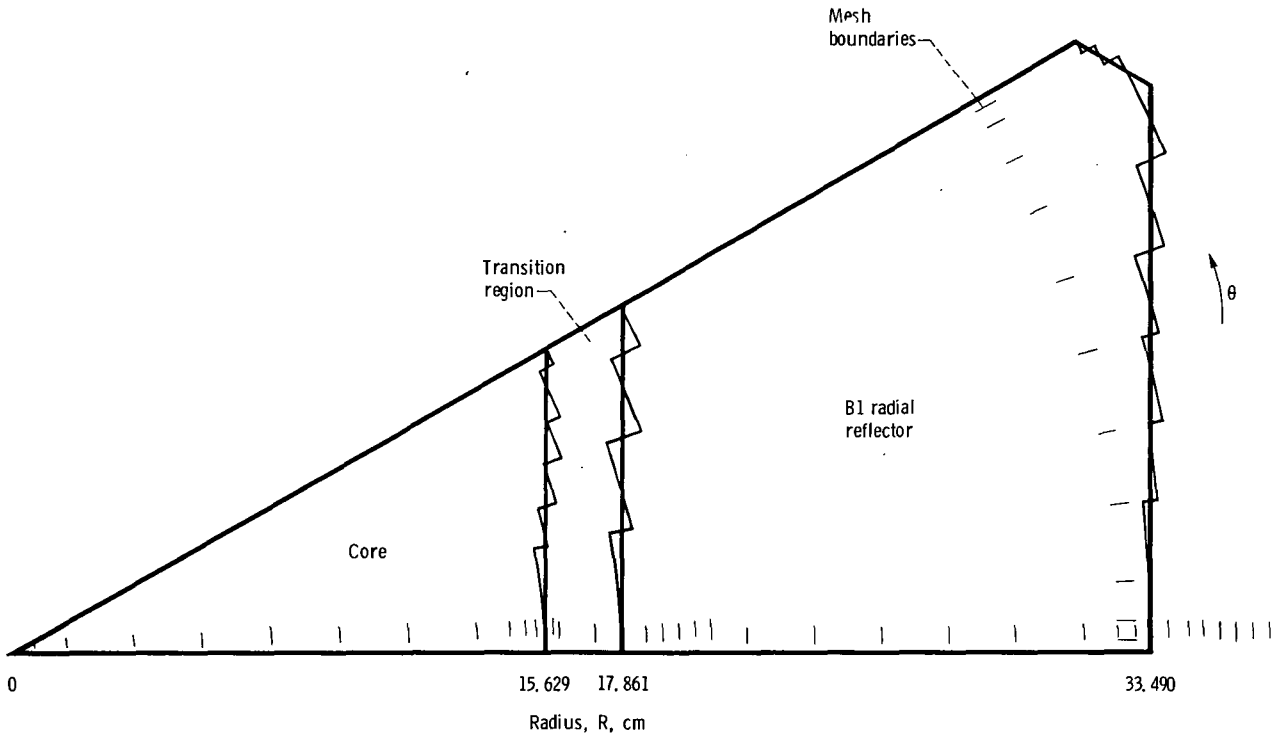

Figure 10. - 30^0 Rθ model geometry.

The use of such a fine mesh is dictated by the sharply rising power peak at the core edge. One-half of the rise of the peak occurs in about the last 0.2 centimeter before the core boundary. A one-dimensional radial model was examined with the mesh intervals near the core edge halved in several steps from the coarse 1-centimeter mesh of the RZ model. These mesh intervals were finally set at the 0.001-centimeter limit in the 67×12 mesh array used in the Rθ model to determine the fineness required in the mesh spacing near the core edge to resolve the size of the power peak. The changes in the mesh spacing for these calculations are shown in figure 11. Calculations of the one-dimensional test models were based on the TRCE B1 configuration using 22-group GAM cross sections. The resulting peaks, as represented by the power calculated in the outermost core mesh interval, are shown in figure 12. The smallest mesh used was the 0.001-centimeter interval. The power peak calculated for this interval was within the ±5 percent error bounds on the measured value.

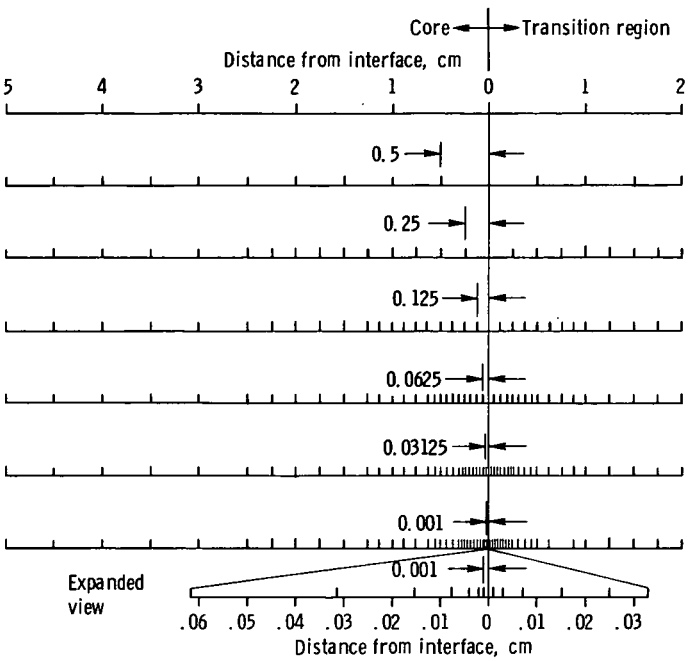

Figure 11. - One-dimensional models for core-edge mesh spacing.

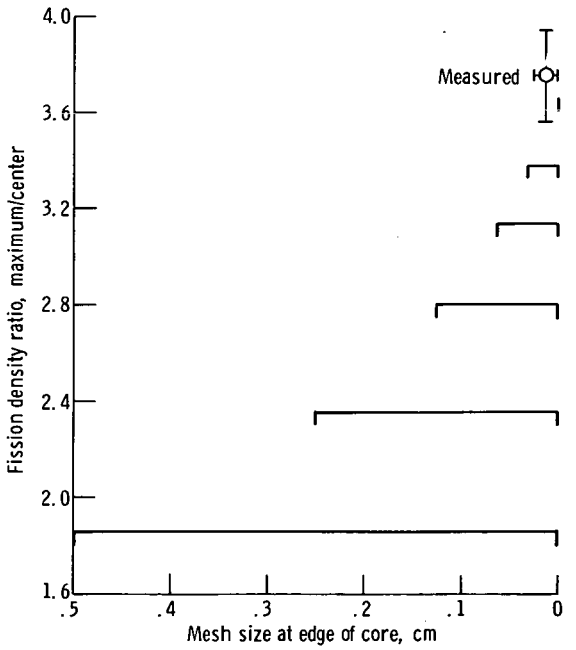

Figure 12. - Mesh-size effect on calculated power peak.

Computing Schemes

Two different schemes were investigated in this study to account for the transverse neutron leakage in the two-dimensional $R\theta$ and one-dimensional radial problems. In one scheme, shown in figure 13, a 24-radial by 25-axial mesh array was used to calculate the whole assembly. Then a one-dimensional model using the same 24 radial mesh intervals was used to iterate on the effective buckling height H_B until the same multiplication factor was obtained in the one-dimensional model as in the RZ model. Then the final H_B was inserted into the fine-meshed (96 radial and 12 azimuthal intervals) radial and $R\theta$ models.

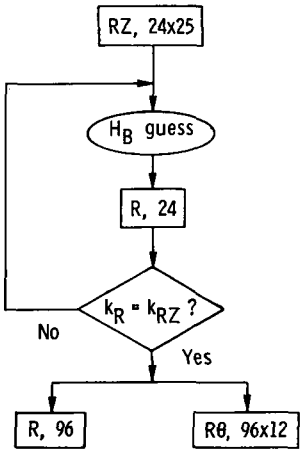

Figure 13. - Computing scheme using effective buckling height.

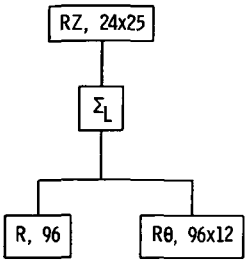

Figure 14. - Computing scheme using effective leakage cross sections.

In the other scheme, shown in figure 14, effective transverse neutron leakage cross sections Σ_L were calculated from the output of a RZ problem. The transverse neutron leakage is related to the transverse buckling by

$$\int \vec{J} \cdot d\vec{S} = \int DB^2 \varphi \, dV \tag{1}$$

where J is the neutron leakage, S is the cross-sectional surface, DB^2 is the transverse buckling, and $\varphi \, dV$ is the incremental volumetric flux. The transverse buckling may also be considered as a transverse leakage cross section, that is,

$$\int DB^2 \varphi \, dV = \int \Sigma_L \varphi \, dV = \bar{\Sigma}_L \int \varphi \, dV \tag{2}$$

or

$$\bar{\Sigma}_L = \frac{\int \vec{J} \cdot d\vec{S}}{\int \varphi \, dV} \tag{3}$$

which says the effective transverse leakage cross section is the ratio of net transverse leakage to total neutron flux. The $\bar{\Sigma}_L$ calculated from equation (3) are included directly into the input of the radial and Rθ problems. The H_B is a single number representing all transverse leakage effects in the assembly, but the Σ_L can be broken down by region and by energy group to be more representative of the different leakage effects in the core and reflector.

RESULTS OF CALCULATIONS

The results of the calculations are discussed here in three parts. First is the base case, the TRCE B1 configuration, which is discussed in more detail than the others. Next, the B2 configuration, with a smaller beryllium reflector than the B1, is discussed, and finally the B1 configuration with the radial beryllium reflector replaced by a beryllium oxide reflector. Two densities of beryllium were used: (1) 2.93 g/cm^3, representing the equivalent replacement density in the experiment using the same volume fraction; and (2) 2.85 g/cm^3, representing the nominal as-manufactured density of beryllium oxide.

Unless otherwise stated, all results presented in this section were obtained by using the cross sections, mostly from the ENDF/B III library, listed in table 8.

TRCE B1 Configuration

The measured value for the neutron multiplication factor k for the TRCE B1 configuration is 1.00103±0.000005 (ref. 1). The calculated values are compared with the measured value in table 11. Data from the RZ calculations were used to calculate the effective buckling height H_B and the effective transverse leakage cross sections Σ_L, by group as well as by region.

The RZ calculations use a coarser mesh than the Rθ calculations; hence, the best values should be found with the Rθ calculations. However, there is a wide range of results in table 11. As a set, the values gained from using Σ_L are much better than

TABLE 11. - MULTIPLICATION FACTORS FROM TWO-DIMENSIONAL CALCULATIONS FOR B1 CALCULATION

Geometry	Number of energy groups	Transverse leakage treatment[a]	Multiplication factor
GAM and GATHER libraries			
RZ	22	-----	1.0189
END/F, GAM and GATHER libraries[b]			
RZ	22	-----	1.0094
	35	-----	1.0124
Rθ	22	H_B	1.0398
		Σ_L-3	1.0035
		Σ_L-12	.9980
		Σ_L-12	[c]1.0110
	35	Σ_L-3	1.0068
		Measured	1.00103

[a] H_B denotes effective buckling height; Σ_L-3 and Σ_L-12 denote effective transverse leakage cross section divided over 3 or 12 zones, respectively.

[b] See table 8.

[c] Be MAT 1007 replaced by Be MAT 1154.

those from H_B, because of the more accurate handling of the effects of the spectrum difference between the core and the reflector. Two radial flux shapes are shown in figure 15 for the 22-group Rθ problem in which a separate set of Σ_L is used in each region (Σ_L-3 in table 11). The overall neutron flux spectrum has two main peaks (listed in table 12): in the 22-group structure, there is a peak in group 6 for the fast flux and one in group 19 for the thermal flux. The mean free paths in these two groups are listed in table 13 and shown in figure 15 for each radial region of TRCE B1. For comparison, the mean free paths of the 2.85-g/cm^3-dense BeO reflector are also listed in table 13. From figure 15 we find that the thermal flux coming into the core from the reflector is essentially absorbed within about three or four mean free paths, or roughly 1 centimeter, which adds the power spike at the edge of the core to an otherwise relatively slowly changing power shape.

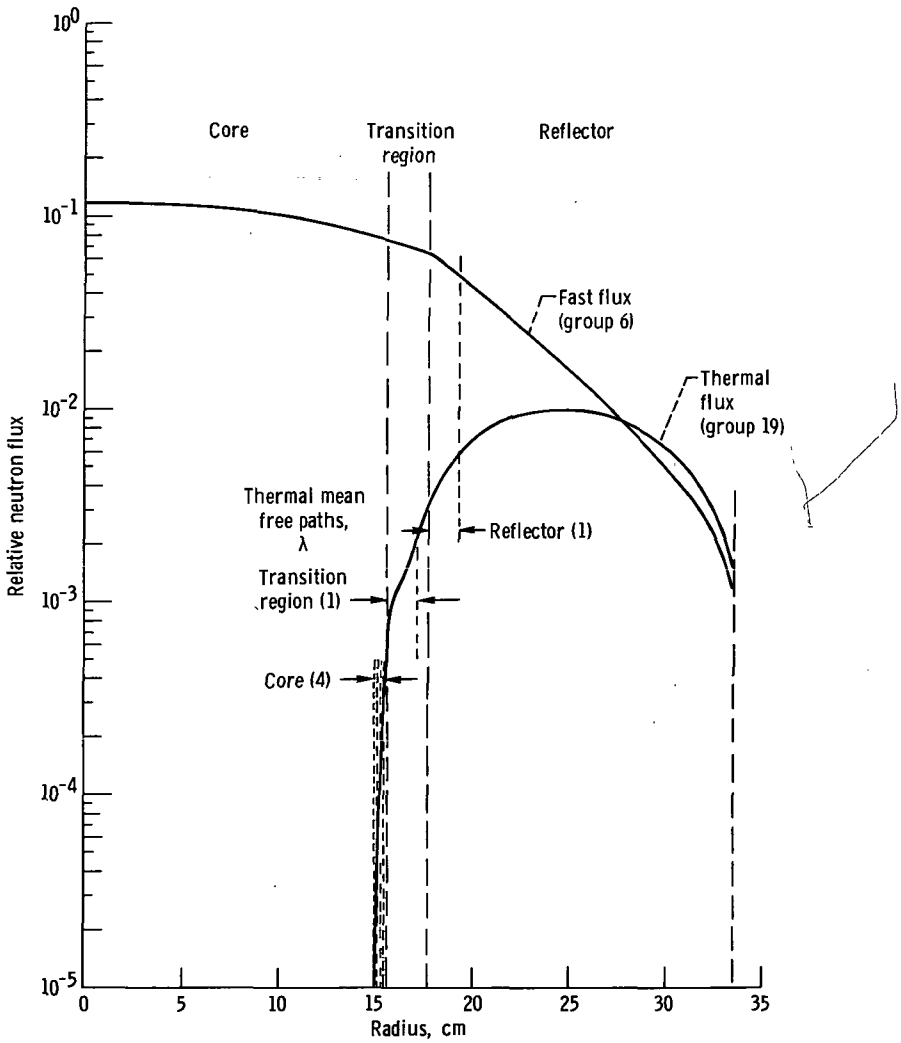

Figure 15. - Radial variation of flux spectrum.

TABLE 12. - B1 CONFIGURATION SPECTRUM

PEAKS FOR 22 GROUPS

	Neutron flux spectrum peaks	
	Fast	Thermal
Group	6	19
Lethargy	3.0 to 4.0	19.34 to 20.03
Energy	498 to 183 keV	0.04 to 0.02 eV

TABLE 13. - B1 CONFIGURATION MEAN FREE PATHS AT

SPECTRUM PEAKS

Region	Total cross section, cm^{-1}		Mean free path, cm	
	Fast	Thermal		
Core	0.310	5.56	3.23	0.180
Transition	.186	.618	5.38	1.62
Be reflector	.463	.681	2.16	1.47
2.85-g/cm^3 BeO reflector	.565	.614	1.77	1.63

To illustrate the difference between the effective-buckling-height H_B and transverse-leakage-cross-section Σ_L methods, the transverse-neutron-leakage rates are plotted in figures 16 and 17 for the core and reflector regions, respectively, from 22-group Rθ problems. Three features stand out in these figures: (1) the Σ_L method allows negative leakages, whereas the H_B does not; (2) the leakage rate integrated over all 22 groups is higher for the Σ_L method than for the H_B method; and (3) in the Σ_L calculations, high-energy leakage is greater and medium- and low-energy leakage is less than in the H_B calculations. The breakpoints at which high-energy leakage is greater in the Σ_L cases are 111 keV for the core and 41 keV for the reflector. The net result is that the more realistic model depicted by the Σ_L method yields a calculated excess reactivity less than one-tenth that from the H_B method, and the result is also only 0.25 percent Δk above the measured multiplication factor. Using 35 groups produces about double the calculated excess reactivity of the corresponding 22-group case. The 35-group calculations consistently yield a slightly higher multiplication factor than do the 22-group calculations. This is evident in all the configurations under study herein.

Using individual group values of Σ_L for each TRCE physical region greatly reduced the error margin in calculating multiplication factors because this method allows

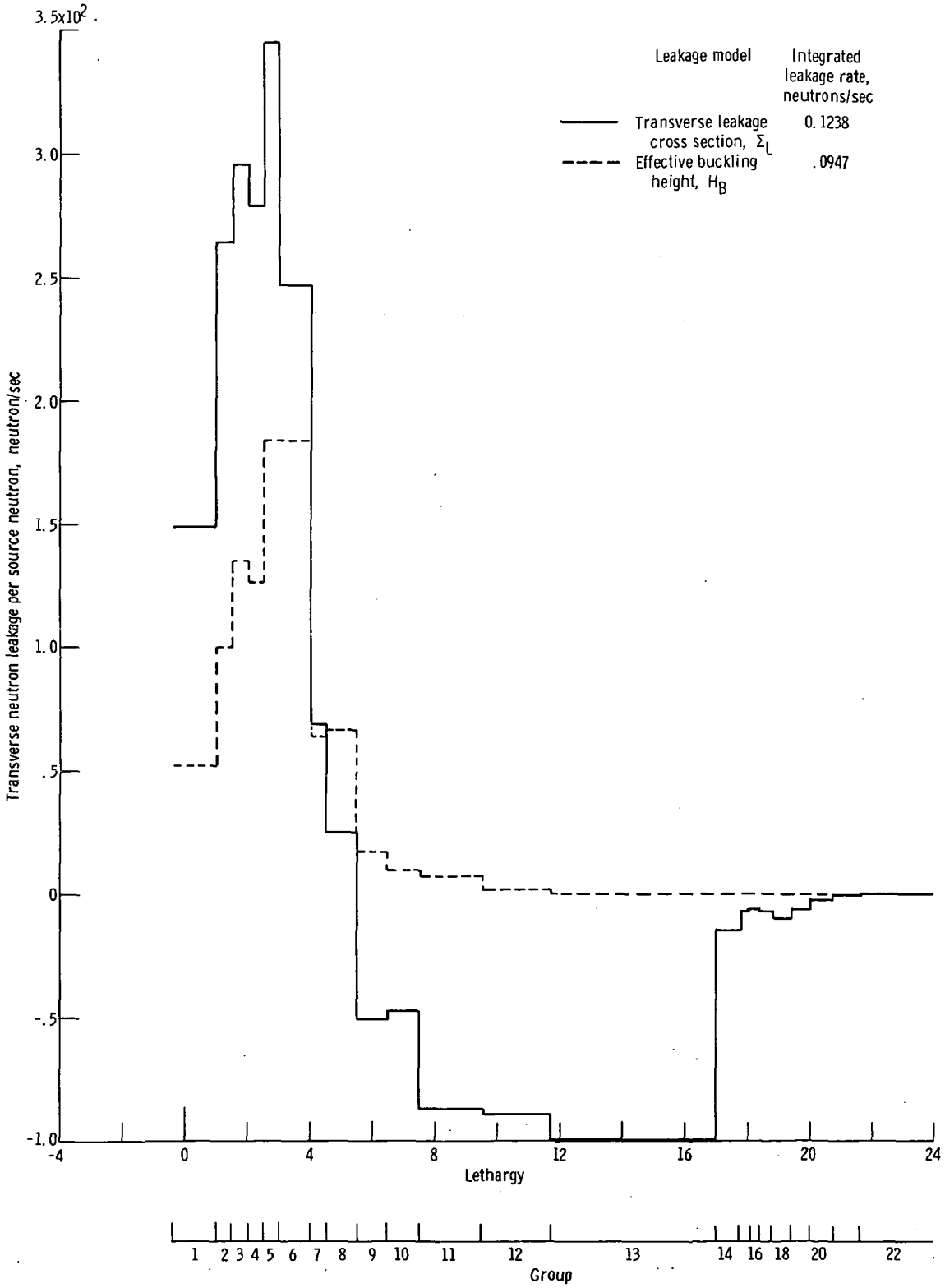

Figure 16. - Transverse leakage in B1 core.

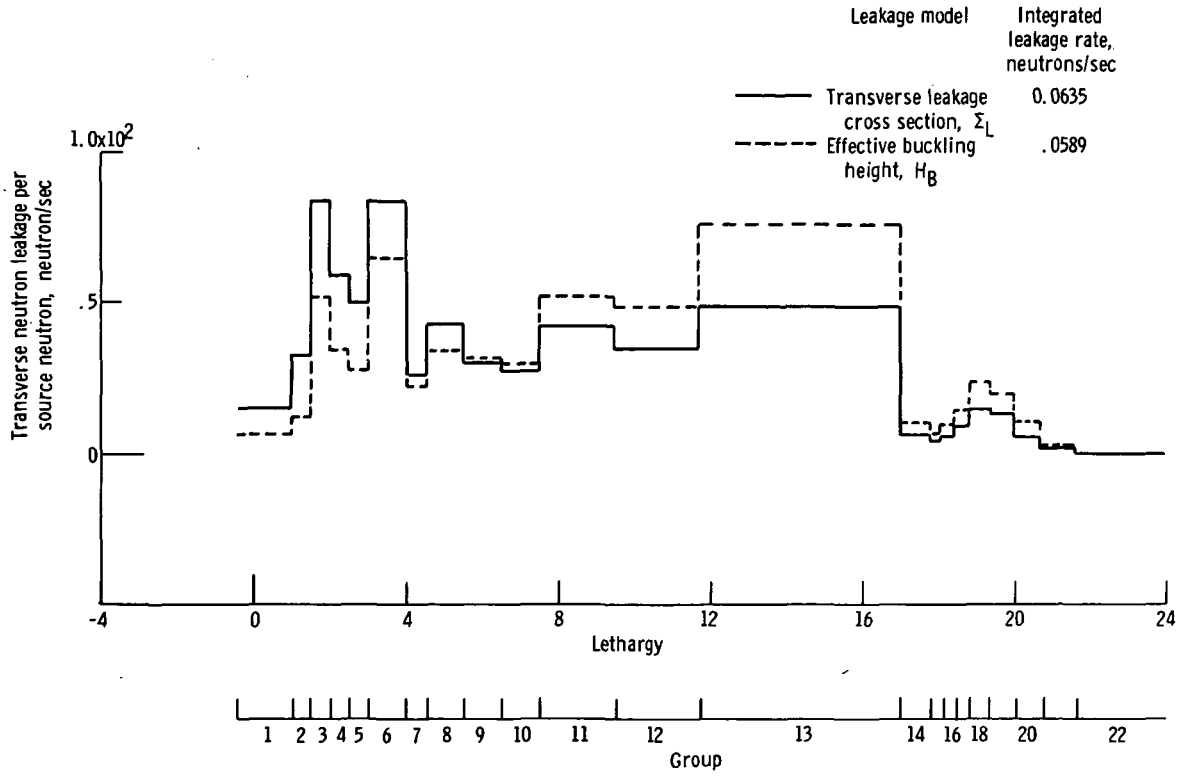

Figure 17. - Transverse leakage in B1 radial reflector.

for the different spectrums found in the core, the transition region, and the reflector. However, in figure 15 it is shown that the spectrum changes significantly within the regions. Hence, the question arises: if using three regions shows a remarkable improvement, would not using a dozen perhaps be even better?

The changes in the relative strengths of the fast and thermal spectrums occur only between about 0.5 centimeter in from the core boundary out to about 6 mean free paths into the reflector, and discrete transverse-leakage cross sections are available from only 24 radial intervals in the RZ model. Therefore, twelve is the optimum maximum number of discrete transverse-leakage subregions that can be calculated in the Rθ model. The subregions are set up in this manner: the core is divided into two subregions, one about 3 to 4 mean free paths wide at the core-transition boundary; the transition is divided into two roughly equal subregions; and the reflector is divided into eight subregions. Three of these subregions are each about 0.5 centimeter wide and are adjacent to the transition-reflector region. They are followed by four more subregions, which are each about 1 centimeter wide, and finally by the outermost subregion, which is about 10 centimeters wide. The 12-subregion model is shown in figure 18.

The result of the calculation was a multiplication factor, 0.9980 (table 11), which is 0.3 percent lower than the measured value. Up to this point all the calculated values have been higher than the measured multiplication factor. A lower value was unexpected

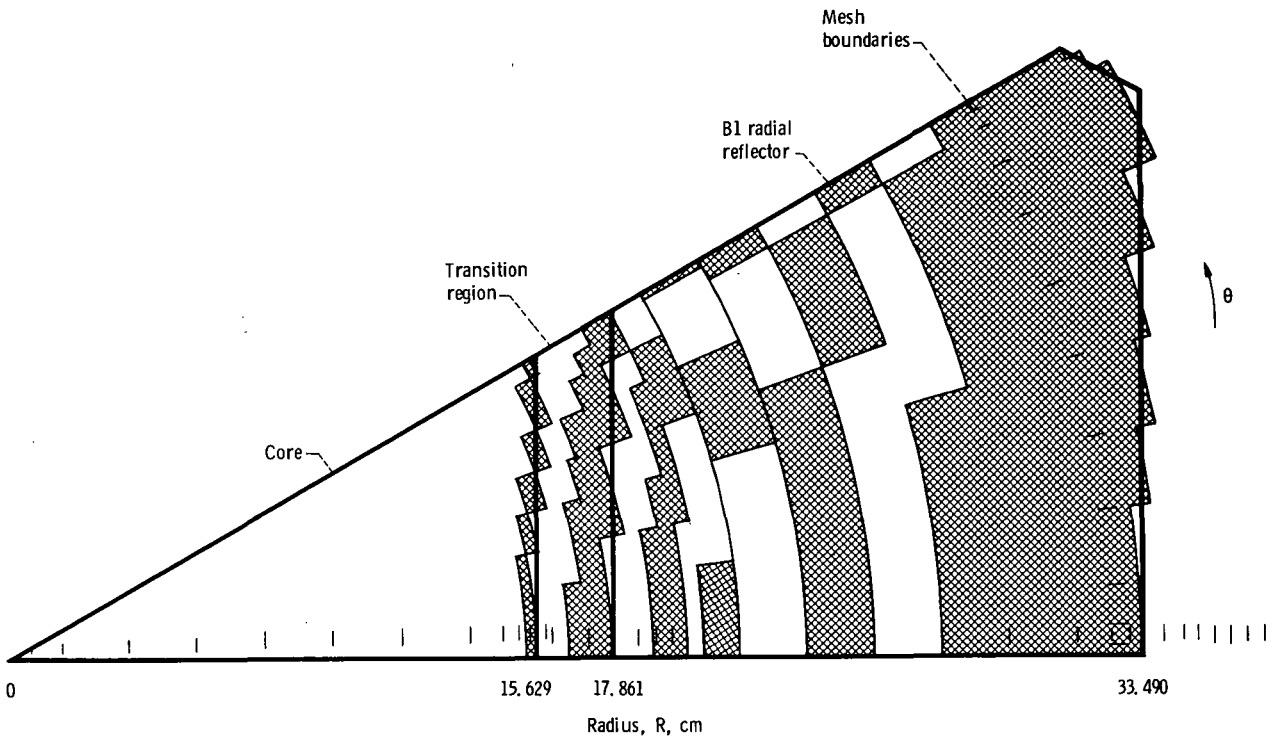

Figure 18. - Twelve-subregion, 30^0 Rθ model geometry.

because a bias was thought to be present due to incorrect leakage treatment. Therefore, another source for the bias must be found. Questions have been raised pertaining to the adequacy of the beryllium cross sections in the ENDF/B II evaluation. Perhaps the ENDF/B III evaluation would provide a better calculation. However, a test using beryllium from ENDF/B III (MAT 1154) in conjunction with GAF/GAR is not possible at this time because of the incompatibility of the form of the data with GAND. The ENDF/B III cross sections are available through SUPERTOG for use with GAM. So a calculation was performed using the materials identified in table 8 with the exception of MAT 1154 for Be. In this calculation, all the fast cross sections were obtained through GAM rather than GAF/GAR. The result for the 12-subregion leakage treatment is 1.0110 for the multiplication factor, which is 1 percent higher than the calculated value. This value is not directly comparable with the others in table 11 because GAM, rather than mostly GAF/GAR, was used for the fast cross sections. It does point out though that there is probably a significant difference between the beryllium cross sections in ENDF/B II and ENDF/B III.

The radial power peak values for the Rθ cases in table 11 are presented in table 14, along with some one-dimensional results from ANISN. A set of representative radial power profiles, for the model given in the first line of table 14 (22-group, S_4RI, H_B) are shown in figure 19. These are not the best of the calculated profiles, but they allow

TABLE 14. - EDGE-TO-CENTER POWER RATIOS IN B1 CONFIGURATION

Computer model			Power peak ratio		
Number of groups	Quadrature[a]	Transverse leakage[b]	One dimensional	Two dimensional, 0^o	$R\theta$, 30^o
22	S_4RI	H_B	3.45	3.18	4.80
	S_4MM	H_B	3.44	-----	-----
	S_8MM	H_B	3.47	-----	-----
	S_4RI	Σ_L-3	3.85	3.45	5.26
	S_4RI	Σ_L-12	----	3.35	5.06
	S_4RI	Σ_L-12	----	[c]3.65	[c]5.50
35	S_4RI	H_B	3.32	-----	-----
	S_4MM	Σ_L-3	3.73	-----	-----
	S_4RI	Σ_L-3	----	3.35	5.06
			Measured	3.75	

[a]RI denotes rotational invariant; MM denotes moment modified.

[b]H_B denotes effective buckling height; Σ_L-3 and Σ_L-12 denote effective transverse leakage cross section divided over 3 or 12 zones, respectively.

[c]Be MAT 1154.

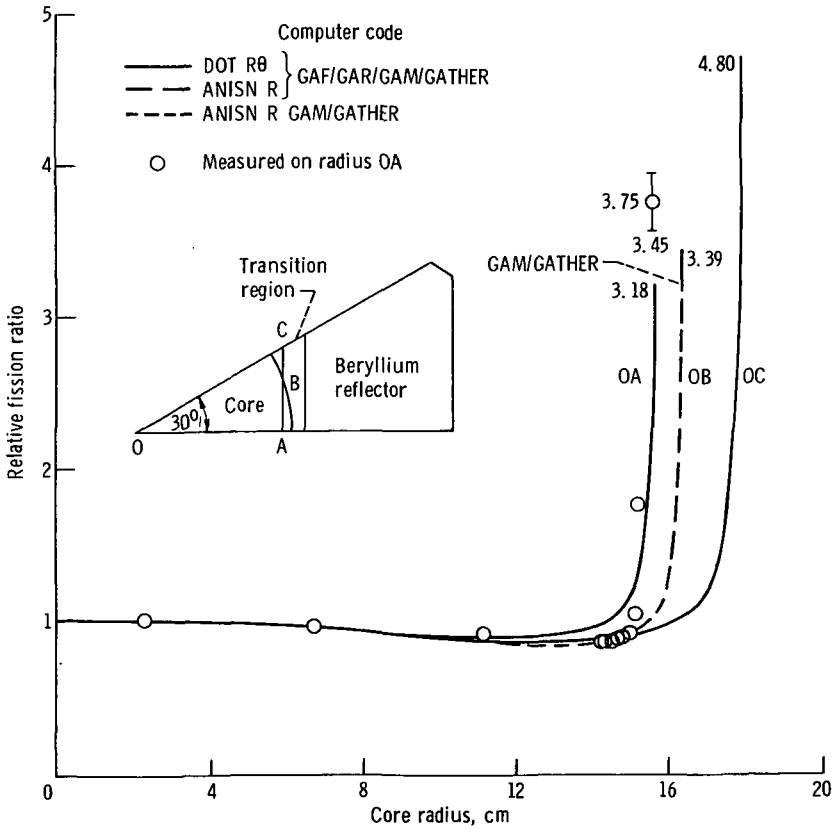

Figure 19. - Radial fission distributions for B1 configuration.

a direct comparison between the use of GAM and GAF/GAR. (GAF/GAR, of course, here means using a set of materials listed in table 8, which does include three materials from GAM.) As in the case of the multiplication factors, using the Σ_L method improves the accuracy of the calculation. Using ENDF/B III beryllium, even though the data is handled through GAM rather than GAF/GAR, yields the only peak calculated within the error bounds on the measured value. The measured peak is 3.75 relative to the power at the center of the core. With a ±5 percent estimated error, the bounds are 3.94 and 3.56. The calculated peak obtained using MAT 1154 for beryllium is 3.65, well within the bounds of the measurement and less than 3 percent below the measured peak.

As shown in figure 19 the peak was measured at the center of the flat, point A. Much higher peaks are found at the apex of the flat, point C in the diagram, because the fuel in the corner sees thermal neutrons returning from a solid angle of beryllium which is 60° larger than at the center of the hexagonal flat. The peak was not measured at point C in the B1 configuration. However, it was in the A configuration, which is very similar in composition. The A configuration has a measured peak at point A (center of flat) of 3.75 in figure 19 and a peak at point C (apex of flat) of 4.80. The peak is considerably higher at the apex of the flat than at the center of the flat; this is also borne out in the calculations. The one-dimensional calculations yield a peak whose value is between the peaks at points A and C. The reason is that in the cylindrical geometry of the one-dimensional calculation, the fuel sees thermal neutrons entering from the reflector at some effective solid angle between that seen by the fuel points A and C in the hexagonal model.

TRCE B2 Configuration

The B2 configuration differs from the B1 configuration mainly by the reduced reflected thickness, from $3\frac{1}{2}$ hexes to 2 hexes, but also by a small increase in oralloy in the core at the expense of Al_2O_3 to keep the measured multiplication factor close to unity.

The measured multiplication factor for B2, 1.001294, is compared with several calculated values in table 15. The H_B method calculates the multiplication factor 2.8 percent Δk too high, and the Σ_L method calculates it 0.7 percent Δk too low. Using 35 groups instead of 22 increases the calculated multiplication factor by about 0.2 percent Δk. The relative accuracy between the H_B and Σ_L methods for the B2 configuration is in general agreement with the B1 results, although the B2 multiplication factor is calculated lower than the measured value in the Σ_L-3 case.

The core-edge power peaks are listed in table 16. In this configuration both apex and center-of-flat peaks were measured. The calculated results were mixed, with center-

TABLE 15. - MULTIPLICATION FACTORS FROM TWO-DIMENSIONAL CALCULATIONS FOR B2 CONFIGURATION

Geometry	Number of energy groups	Transverse leakage treatment[a]	Multiplication factor
RZ	22	-----	1.0026
	35	-----	1.0047
Rθ	22	H_B	1.0292
	22	Σ_L-3	.9940
	35	Σ_L-3	.9962
		Measured	1.001294

[a] H_B denotes effective buckling height; Σ_L-3 denotes effective transverse leakage cross section divided over three zones.

TABLE 16. - EDGE-TO-CENTER POWER RATIOS IN B2 CONFIGURATION

Computer model			Power peak ratio		
Number of groups	Quadrature[a]	Transverse leakage[b]	One dimensional	Two dimensional, 0^0	Rθ, 30^o
22	S_4RI	H_B	1.55	1.48	1.83
	S_4MM	H_B	1.54	-----	----
	S_8MM	H_B	1.56	-----	----
	S_4RI	Σ_L-3	1.78	1.67	2.11
35	S_4RI	H_B	1.40	-----	----
	S_4MM	Σ_L-3	1.63	-----	----
	S_4RI	Σ_L-3	----	1.53	1.88
			Measured	1.506	2.52

[a] RI denotes rotational invariant; MM denotes moment modified.

[b] H_B denotes effective buckling height; Σ_L-3 denotes effective transverse leakage cross section divided over three zones.

TABLE 17. - MULTIPLICATION FACTORS FROM TWO-DIMENSIONAL CALCULATIONS FOR BeO-REFLECTED B1 CONFIGURATION

Geometry	Number of energy groups	Transverse leakage treatment	BeO density, g/cm^3	
			2.93	2.85
			Multiplication factor	
RZ	22	-----	1.0319	1.0279
	35	-----	1.0367	1.0325
Rθ	22	H_B	1.0634	1.0592
	22	Σ_L-3	1.0255	1.0206
	35	Σ_L-3	1.0300	1.0254
		Measured[a]	1.02119	

[a]Measured B1 configuration plus six times measured worth of 1/6 Be reflector replaced with BeO.

of-flat peaks being high and apex-of-flat peaks being too low. Thus, the calculated relative height of the apex-of-flat peak to the center-of-flat peak was substantially lower than the measured value.

TRCE B1 Configuration with BeO Reflector

The beryllium radial reflectors in the B1 and B2 configurations were composed of 0.881 volume fraction of beryllium at 1.85 g/cm^3 and 0.070 volume fraction of aluminum at 2.70 g/cm^3 by volume. In the beryllium oxide substitution experiment, 49 658 grams of beryllium was replaced by 78 605 grams of beryllium oxide in a 60^o sector of the radial reflector. If the volume fractions of Be and BeO were considered to be the same in both cases, this substitution is equivalent to replacing the Be with 2.93-g/cm^3-dense BeO. Usually, BeO is considered to have a nominal 2.85-g/cm^3 density, so calculations were performed using both densities.

Multiplication factors from the calculations are compared with the measured value in table 17. The measured worth of the 60^o sector of beryllium reflector replaced by beryllium oxide was 0.0033 Δk, so the multiplication factor of an entirely beryllium-oxide-reflected B1 configuration should be 1.00103 + 6(0.0033) = 1.02119, the "measured" value shown in table 17. Thus, the H_B method calculates the multiplication factor about 4 percent Δk high, whereas the Σ_L method calculates it only 0.4 percent

Δk high. However, these comparisons of measurement and calculation should only be considered approximate because the reactivity effect may not be linear in extrapolating to full reflector substitution. The calculations also show that the 2.85-g/cm^3-BeO-reflected B1 configuration has 0.5 percent Δk less neutron multiplication than does the 2.93-g/cm^3-BeO-reflected B1 configuration.

Just as the multiplication is reduced when 2.85-g/cm^3-dense BeO is used rather than 2.93-g/cm^3-dense BeO, so are the power peaks, as shown in table 18. Using 22 groups and the Σ_L method yields a very good calculation of the power peak at the center-of-flat core boundary location. At this location the peak is about 4 percent lower in the case of 2.85-g/cm^3 BeO. For purpose of illustration and comparison, radial power shapes for the 2.93-g/cm^3-BeO case using 22 groups and the H_B method are

TABLE 18. - EDGE-TO-CENTER POWER RATIOS IN BeO REFLECTED B1 CONFIGURATION

Computer model			Power peak ratio		
Number of groups	Quadrature[a]	Transverse leakage[b]	One dimensional	Two dimensional, 0°	Rθ, 30°
2.85-g/cm^3 BeO					
22	S_4RI	H_B	2.63	2.47	3.53
	S_4MM	H_B	2.64	-----	----
	S_8MM	H_B	2.66	-----	----
	S_4RI	Σ_L-3	3.00	2.72	3.94
35	S_4RI	H_B	2.51	-----	----
	S_4MM	Σ_L-3	2.86	-----	----
	S_4RI	Σ_L-3	----	2.57	3.73
2.93-g/cm^3 BeO					
22	S_4RI	H_B	2.75	2.55	3.70
	S_4MM	H_B	2.75	-----	----
	S_8MM	H_B	2.77	-----	----
	S_4RI	Σ_L-3	3.13	2.83	4.13
35	S_4RI	H_B	2.62	-----	----
	S_4MM	Σ_L-3	3.00	-----	----
	S_4RI	Σ_L-3	----	2.69	3.93
Measured (2.93-g/cm^3 BeO)				2.836	

[a]RI denotes rotational invariant; MM denotes moment modified.

[b]H_B denotes effective buckling height; Σ_L-3 denotes effective transverse cross section leakage divided over three zones.

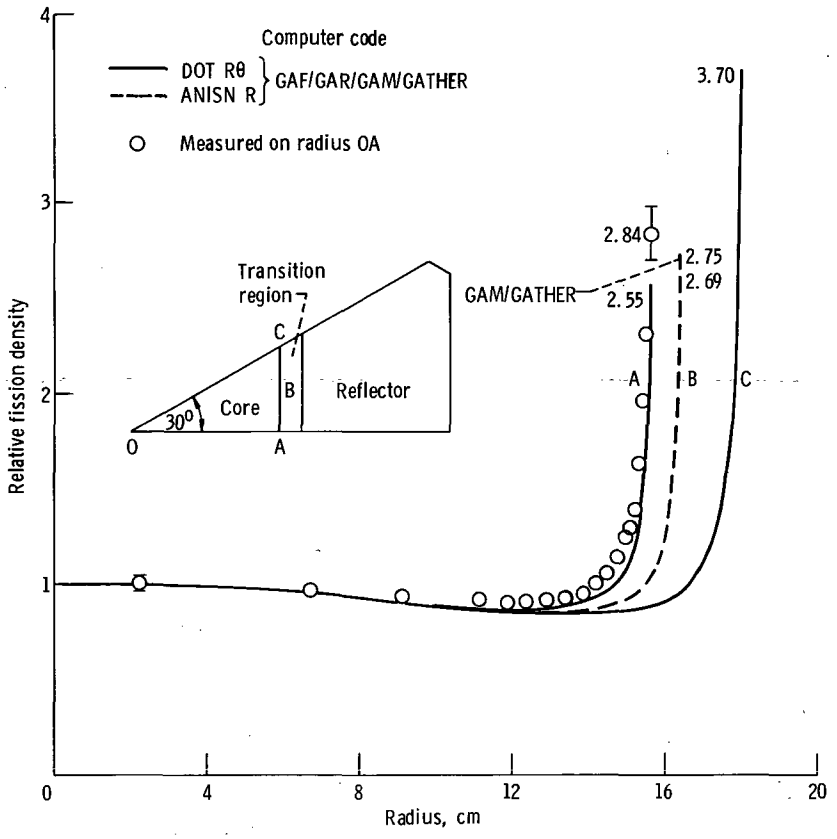

Figure 20. - Fission densities in beryllium-oxide-reflected B1 configuration. Density of BeO, 2.93 g/cm^3; calculation method, effective buckling height H_B.

shown in figure 20 (compare with fig. 19 for the corresponding Be-reflector case). As with figure 19 the same comment appears here: results using the Σ_L method would provide a plot with peaks reaching more closely to the measured peaks, but a direct comparison with GAM/GATHER is shown in the curves in figure 20.

Two examples of the difference between using GAM or GAF/GAR are given in figure 21. The neutron flux spectrums in both cases are nearly the same at the core edge. However, at the center, the lower-energy parts of the spectrums are different, the GAF/GAR cross sections resulting in more neutrons at the lower energies. Another factor in comparing GAM to GAF/GAR is the fission source spectrum present in each of their respective libraries. The fission source spectrums are shown in figure 22. Thus, three factors enter into the difference between using GAM and GAF/GAR:

(1) Fission source spectrum

(2) Microscopic cross-section data

(3) Multigroup cross-section calculation scheme

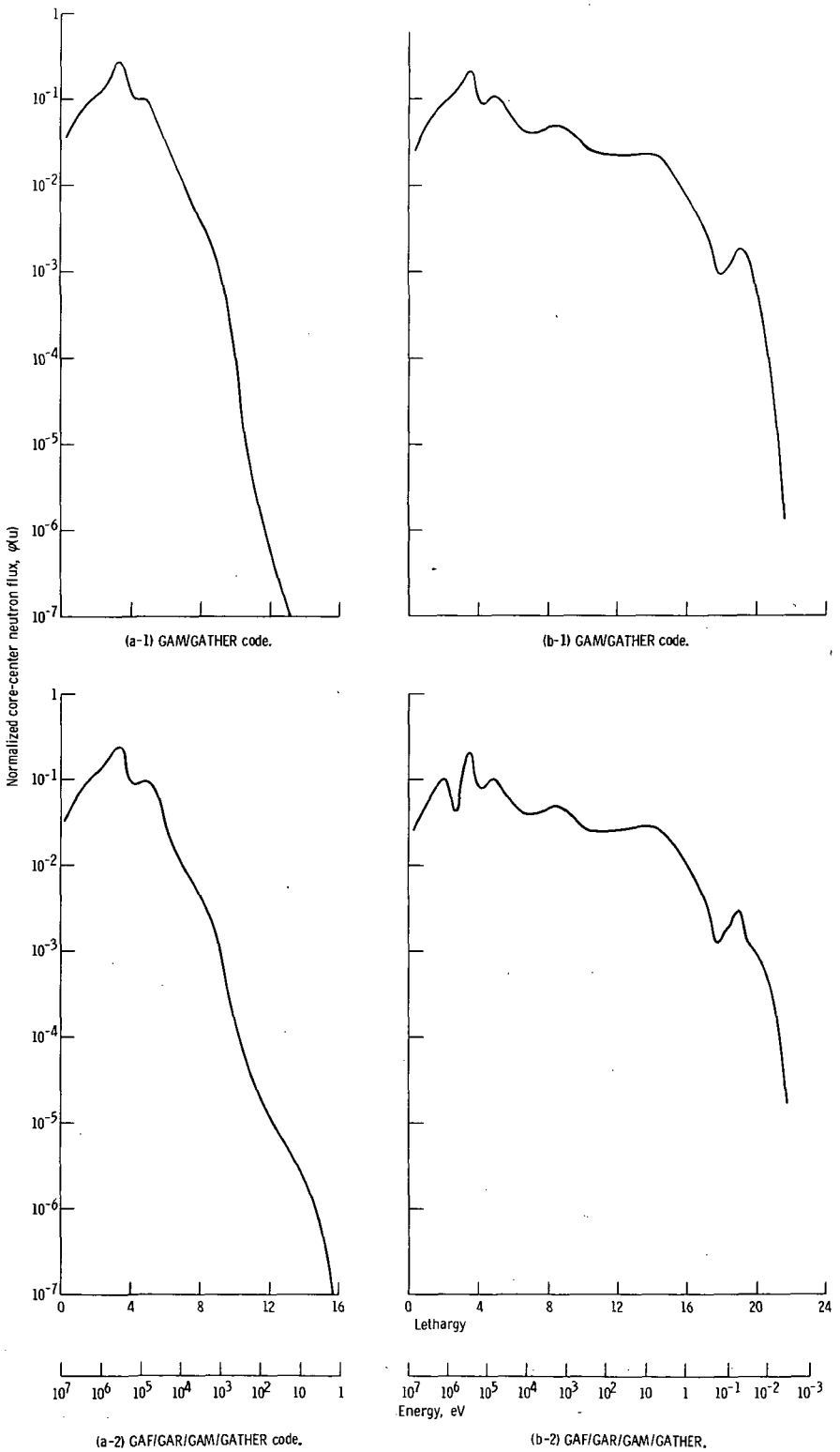

Figure 21. - Flux spectra in beryllium-oxide-reflected B1 configuration. Density of BeO, 2.85 g/cm^3. $\varphi(u)du = 1$.

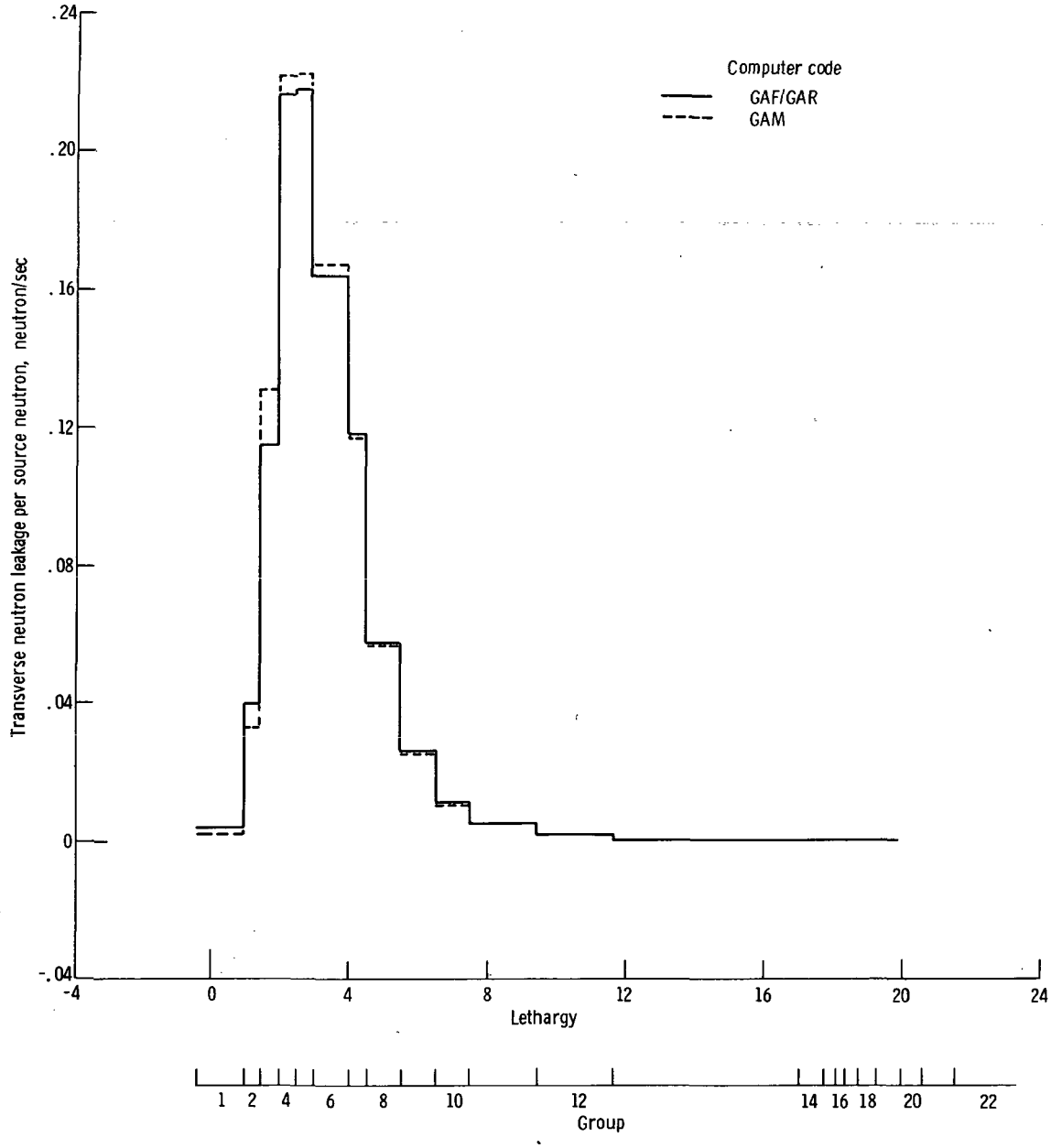

Figure 22. - Fission sources for 22 groups.

Varying Reflector Thickness

Besides the calculations performed to determine biases with respect to measurements in TRCE, some variations on the calculations were also examined to determine a comparative effect of reflector thickness on the Be- and BeO-reflected B1 configuration.

The main thrust of this set of calculations was through one-dimensional radial problems using ANISN. The effect of reflector thickness on neutron multiplication is shown in figure 23. Some two-dimensional RZ problems were also run to check the ANISN calculations at a couple of other reflector thicknesses (6 and 12 cm) in addition to the 16.254-centimeter (cylindrical) B1 radial reflector thickness.

In figure 24 the power peaks, normalized to the core center power, are plotted against radial reflector thickness. Two measured values, for TRCE configurations B1

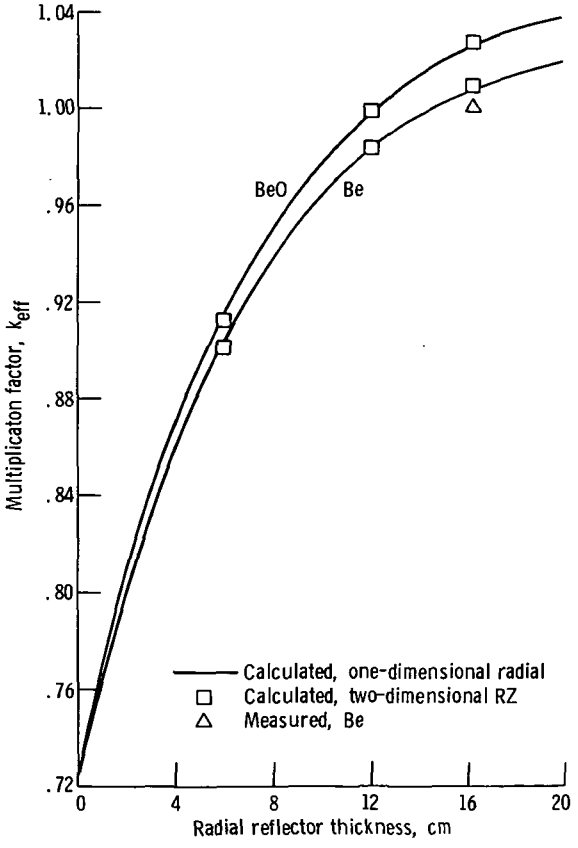

Figure 23. - Effect of reflector thickness on multiplication factor. Density of beryllium oxide, 2.85 g/cm^3.

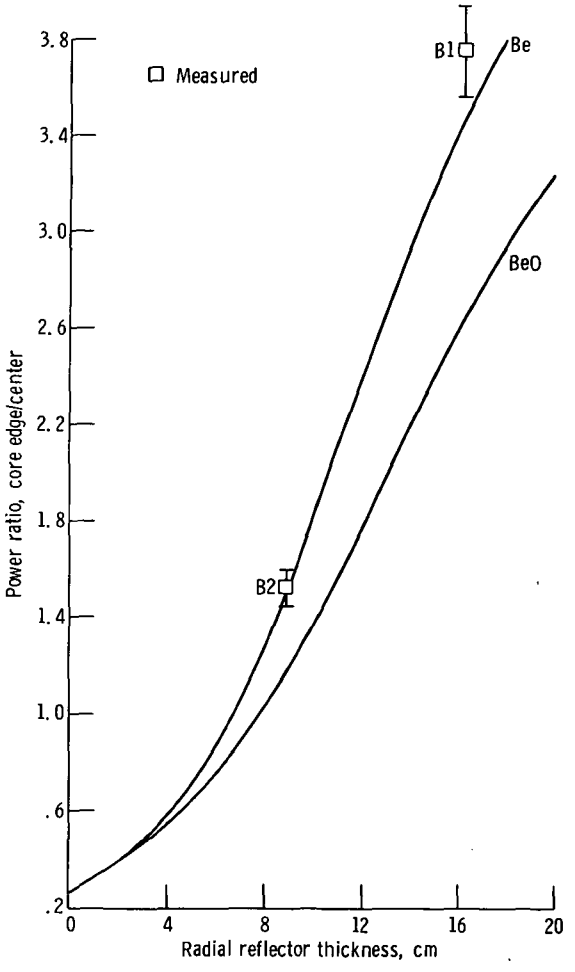

Figure 24. - Effect of reflector thickness on power peak. Density of beryllium oxide, 2.85 g/cm^3.

and B2, are also plotted to indicate the accuracy of the one-dimensional calculations.

Two effects combine to make it advantageous to use a BeO reflector, instead of a Be reflector, with the fast-spectrum TRCE core. First, for the same reflector thickness, BeO causes more multiplication; and, second, for the same reflector thickness, using BeO instead of Be substantially reduces the size of the power peak at the edge of the core (e.g., from 3.4 to 2.6 for a 16-cm reflector). Combine both advantages and we find that instead of a 16-centimeter-thick Be reflector, we can use a 13-centimeter-thick BeO reflector to reduce the power peak from 3.4 to 2.0 and still maintain the same multiplication factor.

DISCUSSION OF REPRESENTATIVE RESULTS

The 22-group set of calculations are the most representative and complete and are thus chosen for discussion here. The effective buckling heights are listed in table 19. The multiplication factors k for all configurations studied are listed in table 20, and their biases in table 21. Normalized peak power factors for all configurations studied are listed in table 22, and their biases in table 23.

The results show that k can be calculated to within about 1 percent accuracy, but it is necessary to use effective transverse neutron leakage cross sections to do so. Using the effective buckling heights gave errors of about 3 and 4 percent, so this method is considered inadequate, at least for reactors with widely different spectrums in the core and reflector. These results are consistent for all three measured configurations.

The power peaking results are not as consistent as the k values: But the results in general, as shown in table 22, are in good agreement with experiment, considering that the accuracy of the measured peaks is ±5 percent. This brings all the peaks calculated by the Σ_L method to within 6 percent of the error allowance of the measured peaks, table 23.

Apex-of-flat power peaks are also listed in table 22, but only one comparison is made with measured values in table 23 because of the lack of measured values. However, some approximate comparisons can be made. The A configuration is similar in composition to the B1 configuration. The B1 configuration has a peak of 3.75 measured at the center of the flat and a peak of 4.80 at the apex; whereas, the corresponding presently calculated values for the B1 configuration are 3.45 and 5.27, respectively (these latter calculations were made by the Σ_L method). Using the same method in the B2 calculation resulted in 1.67 at the center of the flat and 2.11 at the apex. The measured values for B2 are 1.51 and 2.52, respectively. In all cases the Σ_L method produces higher peaks than does the H_B method, and in general the higher peaks are closer to the measured values (including apex and center peaks).

TABLE 19. - EFFECTIVE BUCKLING HEIGHTS

Configuration	Effective buckling height, H_B, cm
B1	64.85
B1 with 2.93-g/cm^3-BeO reflector	65.32
B1 with 2.85-g/cm^3-BeO reflector	65.40
B2	64.27

TABLE 20. - MULTIPLICATION FACTORS

Configuration	Multiplication factor			
	Measured	Calculated[a]		
		RZ	Rθ	
			H_B	Σ_L
B1	1.001030	1.0094	1.0398	1.0035
B1 with 2.93-g/cm^3-BeO reflector	[a]1.02119	1.0094	1.0634	1.0255
B1 with 2.85-g/cm^3-BeO reflector	---------	1.0279	1.0592	1.0206
B2	1.001294	1.0026	1.0292	.9940

[a]H_B denotes effective buckling height; Σ_L denotes effective transverse leakage cross section.

[b]From measured worth of 1/6 BeO reflector, 1.00103 + 6(0.00336).

TABLE 21. - MULTIPLICATION FACTOR BIASES

Configuration	Multiplication factor biases					
	$k_{calc} - k_{meas}$, percent k			$\rho_{calc} - \rho_{meas}$, percent k/k		
	Calculated by RZ	Calculated[a] by Rθ		Calculated by RZ	Calculated[a] by Rθ	
		H_B	Σ_L		H_B	Σ_L
B1	0.837	3.88	0.247	0.828	3.72	0.246
B1 with 2.93-g/cm^3-BeO reflector	1.071	4.22	.431	1.016	3.89	.412
B2	.131	2.79	-.729	.130	2.71	-.733

[a] H_B denotes effective buckling height; Σ_L denotes effective transverse leakage cross section.

TABLE 22. - CENTER-NORMALIZED PEAK POWER FACTORS

Configuration	Power factor		
	Measured	Calculated[a]	
		H_B	Σ_L
Center of flat			
B1	3.751	3.18	3.45
B1 with 2.93-g/cm^3-BeO reflector	2.836	2.55	2.83
B1 with 2.85-g/cm^3-BeO reflector	-----	2.47	2.72
B2	1.506	1.48	1.67
Apex of flat			
B1	-----	4.80	5.27
B1 with 2.93-g/cm^3-BeO reflector	-----	3.70	4.13
B1 with 2.85-g/cm^3-BeO reflector	-----	3.53	3.94
B2	2.52	1.83	2.11

[a] H_B denotes effective buckling height; Σ_L denotes effective transverse leakage cross section.

TABLE 23. - POWER PEAK BIASES

Configuration	Power peak bias, $(P_{calc} - P_{meas})/P_{meas}$, percent	
	Calculated[a] by H_B	Calculated[b] by Σ_L
Center of flat		
B1	-15.22	-8.02
B1 with 2.94-g/cm^3-BeO reflector (ref. 1)	-10.08	-.21
B2	-1.73	10.89
Apex of flat		
B2	-27.4	-16.27

[a] H_B denotes effective buckling height.
[b] Σ_L denotes effective transverse leakage cross section.

CONCLUDING REMARKS

Accurate multigroup transport calculations of mixed test-thermal-spectrum critical assemblies of the Thermionic Reactor Critical Experiment (TRCE) have been made in this report. They require the use of the best available cross-section data, a sophisticated set of cross-section handling codes, large two-dimensional models, and detailed treatment of transverse neutron leakage.

Lewis Research Center,
National Aeronautics and Space Administration,
Cleveland, Ohio, July 24, 1973,
503-25.

REFERENCES

1. Kunze, J. F.; Pincock, G. D.; and Sims, F. L.: Thermionic Reactor Critical Experiment Data Report. Rep. GEMP-423, General Electric Co., Aug. 1966.
2. Joanou, G. D.; and Dudek, J. S.: GAM-II. A B_3 Code for the Calculation of Fast-Neutron Spectra and Associated Multigroup Constants. Rep. GA-4265, General Dynamics Corp., Sept. 16, 1963.

3. Joanou, G. D.; Smith, C. V.; and Vieweg, H. A.: GATHER-II. An IBM-7090 FORTRAN-II Program for the Computation of Thermal-Neutron Spectra and Associated Multigroup Cross Sections. Rep. GA-4132, General Dynamics Corp., July 8, 1963.

4. Honeck, Henry C.: ENDF/B: Specifications for an Evaluated Nuclear Data File for Reactor Applications. Rep. BNL-50066, Brookhaven National Lab., May 1966, Rev. July 1967.

5. Drake, Marvin K.: The ENDF/B Library: A Current Status Report. Proceedings of Conference on New Developments in Reactor Mathematics and Applications. AEC Rep. CONF-710302, Vol. 2, 1971, pp. 991-1003.

6. Archibald, R. J.; and Mathews, D. R.: The GAF/GAR/GAND Fast Reactor Cross Section Preparation System. Vol. I: GAFGAR: A Program for the Calculation of Neutron Spectra and Group-Averaged Cross Sections. Rep. GA-7542, Vol. I, Gulf General Atomic, Inc., Jan. 22, 1968.

7. Mathews, D. R.; and Archibald, R. J.: GAF: A Computer Program for Calculation of Neutron Spectra and Average Cross Sections in the High Energy Region. Rep. GA-7169, General Dynamics Corp., Jan 20, 1967.

8. Stevens, C. A.; and Archibald, R. J.: GAR. A Computer Program for Evaluating Leakage-Dependence Resonance Absorption. Rep. GA-6952, General Atomic, Mar. 1966.

9. Kunze, J. F.; and Sims, F. L.: 710 Basic Critical Experiment Summary Data Report. Rep. GEMP-376, General Electric Co., Dec. 8, 1965.

10. Tipton, C. R., Jr., Ed.: Materials. Vol. 1 of Reactor Handbook. Second ed., Interscience Publ., 1960.

11. Sawyer, Craig: Anslysis of Thermionic Reactor Critical Experiment. Rep. GESR-2078, Vol. II, General Electric Co., Sept. 1966.

12. Anon.: National Neutron Cross Section Center, NNCSC Newsletter No. 72-1, Brookhaven National Lab., Mar. 1972.

13. Anon.: National Neutron Cross Section Center, NNCSC Newsletter No. 71-1, Brookhaven National Lab., Mar. 1971.

14. Wright, R. Q.; Green, N. M.; Lucius, J. L.; and Craven, C. W., Jr.: SUPERTOG: A Program to Generate Fine Group Constants and T_n Scattering Matrices From ENDF/B. ORNL TM-2679, Sept. 1969.

NASA-Langley, 1973 — 22 E-7517

NATIONAL AERONAUTICS AND SPACE ADMINISTRATION
WASHINGTON, D.C. 20546

OFFICIAL BUSINESS
PENALTY FOR PRIVATE USE $300

SPECIAL FOURTH-CLASS RATE
BOOK

POSTAGE AND FEES PAID
NATIONAL AERONAUTICS AND
SPACE ADMINISTRATION
451

U.S.MAIL

POSTMASTER: If Undeliverable (Section 158 Postal Manual) Do Not Return

"The aeronautical and space activities of the United States shall be conducted so as to contribute . . . to the expansion of human knowledge of phenomena in the atmosphere and space. The Administration shall provide for the widest practicable and appropriate dissemination of information concerning its activities and the results thereof."

—NATIONAL AERONAUTICS AND SPACE ACT OF 1958

NASA SCIENTIFIC AND TECHNICAL PUBLICATIONS

TECHNICAL REPORTS: Scientific and technical information considered important, complete, and a lasting contribution to existing knowledge.

TECHNICAL NOTES: Information less broad in scope but nevertheless of importance as a contribution to existing knowledge.

TECHNICAL MEMORANDUMS: Information receiving limited distribution because of preliminary data, security classification, or other reasons. Also includes conference proceedings with either limited or unlimited distribution.

CONTRACTOR REPORTS: Scientific and technical information generated under a NASA contract or grant and considered an important contribution to existing knowledge.

TECHNICAL TRANSLATIONS: Information published in a foreign language considered to merit NASA distribution in English.

SPECIAL PUBLICATIONS: Information derived from or of value to NASA activities. Publications include final reports of major projects, monographs, data compilations, handbooks, sourcebooks, and special bibliographies.

TECHNOLOGY UTILIZATION PUBLICATIONS: Information on technology used by NASA that may be of particular interest in commercial and other non-aerospace applications. Publications include Tech Briefs, Technology Utilization Reports and Technology Surveys.

Details on the availability of these publications may be obtained from:

SCIENTIFIC AND TECHNICAL INFORMATION OFFICE

NATIONAL AERONAUTICS AND SPACE ADMINISTRATION

Washington, D.C. 20546